Review

Anthraquinones-based photocatalysis: A comprehensive review

Cheng-Xin Chen [a], Shan-Shan Yang [a, *], Ji-Wei Pang [b], Lei He [c], Ya-Ni Zang [a], Lan Ding [d], Nan-Qi Ren [a], Jie Ding [a, **]

[a] State Key Laboratory of Urban Water Resource and Environment, School of Environment, Harbin Institute of Technology, Harbin, 150090, China
[b] China Energy Conservation and Environmental Protection Group, CECEP Talroad Technology Co., Ltd., Beijing, 100096, China
[c] CAS Key Laboratory of Urban Pollutant Conversion, Department of Environmental Science and Engineering, University of Science and Technology of China, Hefei, 230026, China
[d] College of Chemistry, Jilin University, 2699 Qianjin Street, Changchun, 130012, China

ARTICLE INFO

ABSTRACT

In recent years, there has been significant interest in photocatalytic technologies utilizing semiconductors and photosensitizers responsive to solar light, owing to their potential for energy and environmental applications. Current efforts are focused on enhancing existing photocatalysts and developing new ones tailored for environmental uses. Anthraquinones (AQs) serve as redox-active electron transfer mediators and photochemically active organic photosensitizers, effectively addressing common issues such as low light utilization and carrier separation efficiency found in conventional semiconductors. AQs offer advantages such as abundant raw materials, controlled preparation, excellent electron transfer capabilities, and photosensitivity, with applications spanning the energy, medical, and environmental sectors. Despite their utility, comprehensive reviews on AQs-based photocatalytic systems in environmental contexts are lacking. In this review, we thoroughly describe the photochemical properties of AQs and their potential applications in photocatalysis, particularly in addressing key environmental challenges like clean energy production, antibacterial action, and pollutant degradation. However, AQs face limitations in practical photocatalytic applications due to their low electrical conductivity and solubility-related secondary contamination. To mitigate these issues, the design and synthesis of graphene-immobilized AQs are highlighted as a solution to enhance practical photocatalytic applications. Additionally, future research directions are proposed to deepen the understanding of AQs' theoretical mechanisms and to provide practical applications for wastewater treatment. This review aims to facilitate mechanistic studies and practical applications of AQs-based photocatalytic technologies and to improve understanding of these technologies.

1. Introduction

Solar energy is an abundant renewable energy source, and photocatalytic technologies employing solar energy and photocatalytic materials show promise in solving environmental problems, particularly water contamination and air pollution [1].

Photocatalysis usually involves light excitation of semiconductors to generate electron (e^-)–hole (h^+) pairs. This is followed by separating and migrating these pairs on the catalyst's surface, leading to photooxidation and photoreduction reactions at the catalytically active site. When the semiconductor photocatalyst absorbs light with energy exceeding its bandgap, e^- migrates from the valence band (VB) to the conduction band (CB), leaving behind h^+ in the VB. On the surface of the photocatalyst, e^- reduces oxygen (O_2) to generate superoxide radicals $(O_2^{\bullet-})$, while h^+ oxidizes H_2O or OH^- to generate hydroxyl radicals $(^{\bullet}OH)$, thereby minimizing the recombination of e^- and h^+. Thus, the e^- in the CB and h^+ in the VB can reduce and oxidize contaminants adsorbed on the photocatalyst surface. Photocatalytic technology can treat a wide range of contaminants, encompassing pharmaceutical and personal care

* Corresponding author.
** Corresponding author.
E-mail addresses: shanshanyang@hit.edu.cn (S.-S. Yang), dingjie123@hit.edu.cn (J. Ding).

Abbreviations

$^1AQ^*$	Singlet excited state of AQ
$^3(AQ\text{-}X)^{*-}$	Charge transfer binary exciplex intermediate
$^3AQ^*$	Triplet excited state of AQ
A	Acceptor
AHQ	Anthrahydroquinone
AQ	9,10-Anthraquinone
$AQ^{\bullet-}$	Anthraquinone radical anion
AQ2S	Anthraquinone-2-sulphonate
AQ-COOH	Anthraquinone-2-carboxylic acid
AQs	Anthraquinones
ASC	Anthraquinone-2-sulfonyl chloride
CB	Conduction band
CDOM	Chromophoric dissolved organic matter
COF	Covalent organic framework
D	Donor
DAAQ	2,6-Diaminoanthraquinone
DAHA	1,5-Diamino-4,8-dihydroxyanthraquinone
DCIP	2,6-Dichloroindophenol
DFT	Density functional theory
DNA	Deoxyribonucleic acid
E. coli	*Escherichia coli*
GC	Glassy carbon
g-C_3N_4	Graphitic carbon nitride
GO	Graphene oxide
HOMO	Highest occupied molecular orbital
H_2	Hydrogen
H_2O_2	Hydrogen peroxide
HAp	Hydroxyapatite
HAT	Hydrogen atom transfer
IBP	Ibuprofen
ICT	Intermolecular charge transfer
ISC	Intersystem crossing
LED	Light-emitting diode
LUMO	Lowest unoccupied molecular orbital
MOF	Metal-organic framework
$^1O_2$	Singlet oxygen
$O_2^{\bullet-}$	Superoxide radicals
OER	Oxygen evolution reaction
$^{\bullet}OH$	Hydroxyl radicals
ORR	Oxygen reduction reaction
PCET	Proton-coupled electron transfer
PDT	Photodynamic therapy
PEC	Photoelectrochemical
PP	Purpurin
PUF	Polyurethane foam
rGO and RGO	Reduced graphene oxide
ROS	Reactive oxygen species
S. aureus	*Staphylococcus aureus*
XRD	X-ray diffraction
TD-DFT	Time-dependent DFT
T. denitrificans	Thiobacillus denitrificans
TiO_2	Titanium dioxide
UVA	Ultraviolet A
VB	Valence band
X^-	Halide ions
XPS	X-ray photoelectron spectroscopy

products, dyes, pesticides, microplastics, heavy metals (Cr, Hg, and Pb), harmful algal, and inorganic salts, such as nitrate (NO_3^-) [2–7].

Ideal photocatalytic materials are important for photocatalytic technology; they should be low-cost, non-toxic, derived from abundant raw materials, highly efficient, stable, easy to separate and recover, and capable of effectively absorbing visible light. Titanium dioxide (TiO_2) is a commonly discussed semiconductor photocatalyst due to its affordability and unique photochemical properties [8]. However, limited light utilization and high photo-generated e^-–h^+ pairs recombination are major obstacles to TiO_2-based photocatalysis technology [9]. Thus, researchers have developed and applied various photocatalytic materials, including metal oxides [10], Bismuth oxyhalide [11], conjugated microporous polymers [12], metal-organic frameworks (MOFs) [13], graphitic carbon nitride (g-C_3N_4) [14], covalent organic frameworks (COFs)

[15], anthraquinones (AQs) [16], plasmonic metal nanostructures (Au, Ag) [17], perovskite [18], and self-assembled supramolecules, such as perylene imide [19], porphyrin [20], and phthalocyanine [21]. These photocatalytic materials are employed for diverse applications, such as organic pollutant degradation and heavy metal detoxification. For instance, Yan et al. [22] constructed a $ZnFe_2O_4$/Bi_2S_3 heterojunction for antibiotic decomposition and heavy metal ion detoxification in water, achieving 91.6% tetracycline degradation and 96.7% Cr(VI) reduction within 2 h of visible light irradiation. Greco et al. [23] reported a $Co_3O_4@Co(OH)_2$ photocatalytic composite capable of degrading 40% of polystyrene microplastics under whit light-emitting diode (LED) illumination, with a hydrogen (H_2) production efficiency of 43 μmol g^{-1} in the absence of a sacrificial agent with $Co_3O_4@Co(OH)_2$. Yue et al. [24] developed MOFs featuring Cu nodes, demonstrating exceptional photocatalytic inactivation of *Microcystis aeruginosa* and microcystin degradation.

Among the numerous types of photocatalysts, non-metal photocatalysts, such as g-C_3N_4 and AQs, have recently garnered significant attention in the field [1,25–27]. AQs are naturally occurring quinone compounds commonly found in plants and serve as natural colorants [28]. AQs are recognized for their remarkable electron transfer capabilities, functioning as redox mediators that enhance the anaerobic bioreduction of heavy metals and organic pollutants [29,30]. Owing to their electrochemical activity, AQs also find application as electrode materials in supercapacitors and batteries, including lithium-ion and aluminum-ion batteries [31,32]. The photochemical properties of AQs, particularly sulfate derivatives, have garnered attention due to their ability to effectively absorb ultraviolet (UV) and visible light, with tunable photoredox characteristics achievable through molecular structure design [33–36]. For example, under suitable wavelengths, 9,10-anthraquinone (AQ) undergoes a rapid transition from its ground state to an excited state, leading to the formation of a semiquinone radical ($AQH^{\bullet}$) through hydrogen abstraction, ultimately resulting in the production of anthrahydroquinone (AHQ). By introducing O_2 into the AHQ solution, hydrogen peroxide (H_2O_2) can be generated, subsequently regenerating AQ. During photoinduced single-electron transfer processes, AQ generates a radical anion ($AQ^{\bullet-}$) capable of transferring electrons to aryl halides [37].

Due to their unique photochemical properties, AQs have been extensively studied for various applications, including high-value chemical photosynthesis, textile dyeing, photocatalytic H_2O_2 production, photodynamic therapy (PDT), photocatalytic pollutant degradation, and sterilization [26,28,38–42]. Despite their advantages, AQs have peculiar challenges, such as low electronic conductivity, photogenerated carrier recombination, and poor recoverability [43]. To overcome these limitations, AQs are often anchored to inert carriers, photocatalysts, or cocatalysts with high electron transfer capabilities [1,16]. For example, AQs modification of graphene surfaces can improve light-induced bactericidal and pollutant degradation [1,40].

AQs have been extensively investigated for their optical properties and applications for many years. Some researchers have comprehensively reviewed various aspects of AQs, including photocatalytic organic transformations, PDT, photoinitiators for polymerization, and chemosensors [28,44–47]. However, to date, limited reviews have focused on the role of AQs as photocatalysts for environmental applications, encompassing energy conversion and pollutant degradation. Therefore, this review summarizes the advancements in photochemical research on AQs, highlighting their distinctive redox properties and photocatalytic characteristics. The advantages of AQs-based photocatalytic technologies across various fields are elucidated. Relevant published articles were identified using keywords related to anthraquinone,

photocatalysis, photosensitivity, anchoring, and modification. The primary objectives of this review include discussing (i) the photochemical characterization of AQs, (ii) the environmental applications of AQs in the realm of photocatalysis and photochemistry, and (iii) various immobilization strategies for AQs. Finally, we provide a perspective on future research directions in related fields. This review offers novel insights into designing and developing efficient AQs-based photocatalytic systems tailored to environmental applications.

2. Optical properties and photochemical principles of AQs

2.1. Photochemical properties

AQ is a macrocyclic conjugated aromatic compound featuring carbonyl groups at positions 9 and 10, characterized by the molecular formula $C_{14}H_8O_2$ [28]. Table 1 presents the structures of the commonly studied AQs. Due to the presence of two carbonyl groups in its ring structure, AQs exhibit a strong electron-accepting capability. AQs also display various functional groups and electronic properties, exhibiting different physicochemical properties. As shown in Fig. 1, upon exposure to light of an appropriate wavelength, AQ absorbs light energy, transitioning from its ground state to a singlet excited state ($^1AQ^*$) [48]. Electrons within the transient $^1AQ^*$ can transition to a longer-lived, albeit lower-energy, triplet excited state ($^3AQ^*$) and undergo spin conversion through intersystem crossing (ISC) [48–50]. $^3AQ^*$ can convert triplet oxygen ($^3O_2$) into reactive oxygen species (ROS) through two primary photooxidation mechanisms. The type I reaction proceeds through an electron-transfer mechanism: upon excitation by light at a suitable wavelength, $^3AQ^*$ is reduced by the substrate to generate $AQ^{\bullet-}$, subsequently engaging with molecular oxygen to yield $O_2^{\bullet-}$ or $^\bullet OH$ [49,51,52]. Type II reactions entail the generation of excited singlet oxygen ($^1O_2$) via energy transfer processes [51]. Generally, the effectiveness of these mechanisms may be influenced by the catalyst structure, substrate, and reaction conditions.

2.2. Electron properties of AQs

Density functional theory (DFT) is an effective method to investigate molecules' electronic properties. We applied DFT calculations to analyze 11 AQs, as shown in Table 1. The calculations were performed using Gaussian16 to optimize the AQs' ground and triplet state geometries [53,54]. Geometry optimizations and vibrational frequency calculations were performed at the B3LYP functional [55,56] with D3 (BJ) dispersion corrections [57] on a 6-31G (d, p) basis set using the polarizable continuum model (PCM) [58,59] as a solvent model and water as the solvent. The excited states were calculated using time-dependent DFT (TD-DFT).

The different highest occupied molecular orbital (HOMO) and lowest unoccupied molecular orbital (LUMO) energy levels for these AQs are due to the varying electron-donating/withdrawing groups attached to the AQ structure. These substituents modulate the AQ's molecular orbital energy level and redox capacity. For example, AQs with electron-withdrawing groups (such as −COOH, −SO_3H, and −Cl) exhibit stronger redox capacities [60]. Table 1 shows the variations in the HOMO−LUMO gap (the energy difference between the HOMO and LUMO energy levels) of the AQs. The HOMO−LUMO gap decreases with the introduction of either electron-donating or electron-withdrawing substituents on the AQ skeleton, a finding experimentally validated by Jiang et al. [25]. Further, the HOMO−LUMO gap tends to decrease with an increase in the number of groups. Notably, 1-aminoanthraquinone and 1,5-diaminoanthraquinone has the narrowest HOMO−LUMO gap among the 11 AQs, with 3.05 and 3.02 eV, respectively (Table 1). In

general, a smaller energy gap facilitates electron transitions with less energy absorption, enabling easier excitation of electrons and favoring absorption of longer wavelengths of sunlight.

In terms of light-absorbing ability, the introduction of electron-donating groups (e.g., −NH_2 and −OH) to an AQ molecule results in a redshift in its light absorption range by affecting the electronic states and transitions of the AQ (Table 1) [28]. Intramolecular and intermolecular hydrogen bonds [61], conjugated effects [62], and steric hindrance effects [63] between substituents and AQ also play crucial roles. For example, hydroxyl groups in 1-hydroxyanthraquinone contribute to increased conjugation length through a resonance effect, resulting in a redshift in the absorption spectrum [64]. Substituent-induced attenuation in the photoluminescence spectra indicates greater stability of the photoexcited state of substituted AQ [64]. Relative to AQ, substituent groups lower the excitation energy, reduce HOMO−LUMO gaps, and promote electron excitation and transfer.
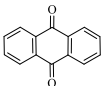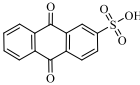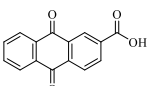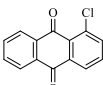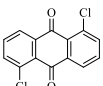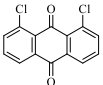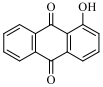
Several AQs have been investigated for photocatalytic applications under solar light exposure, with substituents influencing electron and/or proton transfer reactions [65]. For instance, replacing a hydrogen atom in AQ with a halogen atom enhances the photocatalytic oxidation activity of aromatic alcohols [66]. Halogen substitution increases the quantum yield ratio of phosphorescence to fluorescence, indicating a higher number of triplet-state molecules, enhanced redox capacity, and increased photocatalytic reactivity. Furthermore, given their favorable redox activity, AQs incorporated into materials to form composites serve as conductive channels that spatially separa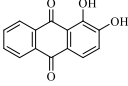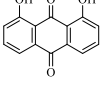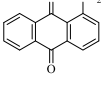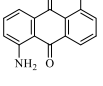te charges and prolong the lifetime of photogenerated carriers. AQs can also act as electron acceptors in donor (D)–acceptor (A) conjugated polymers. The electron-deficient nature of the AQ units facilitates intramolecular charge transfer, generating a built-in electric field that promotes carrier migration. Compared to an anthracene unit, D–A polymers with AQ units exhibit lower LUMO positions, narrower band gaps, enhanced visible-light absorption, and improved photocatalytic activity [26]. These structural variations significantly influence the redox capacity and photocatalytic performance of AQs.

2.3. Light-driven generation of ROS

As indicated in Section 2.1 regarding the photochemical behavior of AQs, they can generate diverse ROS, including $^\bullet OH$, $O_2^{\bullet-}$, $^1O_2$, and H_2O_2. These ROS exhibit vigorous redox activity, and the production of ROS is paramount for applications in energy conversion and environmental remediation. AQs bearing different substituents manifest distinct electronic configurations and ROS generation capabilities [67]. For instance, DFT studies by Liu et al. [68] revealed that anthraquinone-2-sulphonate (AQ2S) exhibited a higher formation energy for triplet excited states compared to disubstituted AQ, enhancing its capacity to abstract hydrogen and react with O_2 to yield ROS. The nature of ROS generated during photocatalysis is significantly influenced by the characteristics of the reaction medium and the electron-donating properties of the substrate [69]. For example, the interaction between water and photoexcited AQs leads to the formation of a quinone-water exciplex, subsequently yielding $O_2^{\bullet-}$ and H_2O_2 upon reaction with O_2 [70].

A study exploring the photocatalytic $^1O_2$ production capacity of AQs found that AQ-2-carboxylic acid (AQ-COOH) exhibited a quantum yield of 0.76 for $^1O_2$ production in acetonitrile solution, determined using rubrene as a selective probe and perinaphthenone as a reference photosensitizer [71]. The quantum yield of $^1O_2$ production by AQ is about 0.17 in a benzene solution [72]. Considering the low fluorescence quantum efficiency of the AQs, this suggests that the transition from the singlet to the triplet state

Table 1
The common structures and electron properties of AQ and its derivates by DFT calculations.

Name	Structure	HOMO (eV)[a]	LUMO (eV)[a]	HOMO−LUMO gap (eV)	Absorption maxima (λ_{max}^{abs}, nm)[b]	Triplet excited state energy (eV)[b]
9,10-Anthraquinone		−7.16	−2.92	4.25	413	2.33
Anthraquinone-2-sulfonate		−7.40	−3.20	4.20	418	2.06
Annthraquinone-2-carboxylic acid		−7.29	−3.11	4.18	419	2.08
1-Chloroanthraquinone		−7.07	−3.01	4.06	434	1.69
1,5-Dichloroanthraquinone		−7.05	−3.09	3.96	446	1.68
1,8-Dichloroanthraquinone		−7.09	−3.03	4.05	432	1.45
1-Hydroxyanthraquinone		−6.53	−3.04	3.49	414	0.74
1,2-Dihydroxyanthraquinone		−6.22	−2.98	3.25	439	0.51
1,8-Dihydroxyanthraquinone		−6.48	−3.13	3.35	435	0.82
1-Aminoanthraquinone		−5.83	−2.78	3.05	473	1.30
1,5-Diaminoanthraquinone		−5.66	−2.65	3.02	480	1.39

Abbreviations: HOMO, highest occupied molecular orbital. LUMO, lowest unoccupied molecular orbital.
[a] Calculated by DFT.
[b] TD-DFT.

promotes the formation of $^1O_2$. −OH substitution at position 1 on AQ enhances $^1O_2$ quantum yield compared to −OCH$_3$ substitution at position 1 on trisubstituted AQ [51]. The quantum yield for $^1O_2$ production by −OCH$_3$ substituted AQ is enhanced significantly when neighboring positions (e.g., position 2) are occupied by −CHO or −CH$_2$OH groups. The −CHO and −CH$_2$OH functional groups can counteract the decreasing effect of the −OCH$_3$ group [51]. This phenomenon can be attributed to alterations in the triplet excited state configuration induced by strong electron-donating substituents [73]. Furfuryl alcohol (FFA) is a commonly used probe for $^1O_2$ detection. Notably, using FFA in complex photochemical reactions can misestimate $^1O_2$ quantum yields when other ROS and electron transfer are present [69].

Regarding photocatalytic $^\bullet$OH production, the ability of AQs to produce $^\bullet$OH varies with the characteristics of the substituents. Monosubstituted AQs featuring hydroxyl or amino groups at position 1 or 2 exhibit reduced $^\bullet$OH yield due to intramolecular hydrogen bonding. By contrast, AQs bearing electron-withdrawing or weakly electron-donating groups, such as alkyl, carboxyl, and sulfonic acid groups, at position 2 demonstrate enhanced $^\bullet$OH production [73]. This phenomenon can be attributed to the formation of hydrogen bond, affecting the radiation-free deactivation of the singlet excited state of AQs, thus reducing their photoactivity and ROS yield [74]. Intramolecular charge transfer and solvent polarity also contribute to the low $^\bullet$OH efficiency of 2-hydroxyanthraquinone [73]. Similarly, the production of H$_2$O$_2$ by
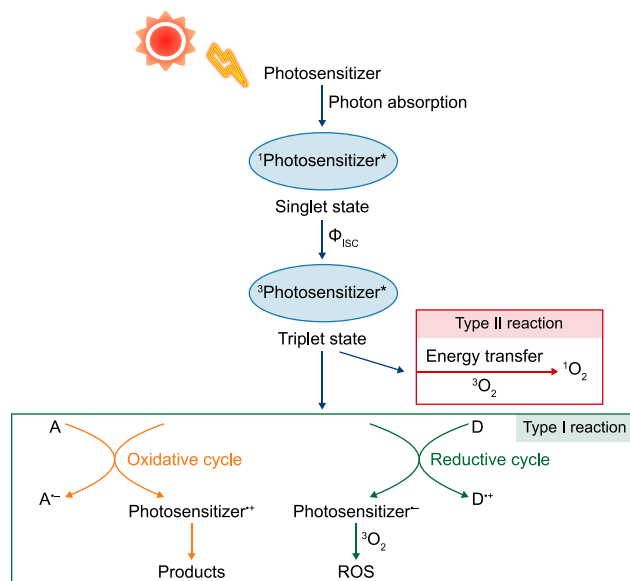
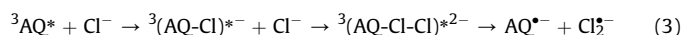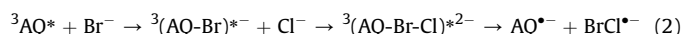**Fig. 1.** The photosensitization processes of organic photosensitizer.

AQs is influenced by substituent type, with carboxyl, *tert*-butyl, methyl, unsubstituted, and chlorine groups ranked in order of increasing H_2O_2 production efficiency [75]. In addition to ROS generation in the homogeneous phase, AQs loaded onto solid-phase matrices offer promising applications in photocatalysis for pollutant degradation and antibacterial activity, utilizing their light-driven ROS-generation properties [76–78]. For example, in a D–A conjugated polymer photocatalytic system, the reaction of AQs radical anions with O_2 promotes $O_2^{\bullet-}$ [26]. In brief, the diverse ROS production capabilities of AQs stem from variations in redox potentials, triplet quantum yields, intermolecular hydrogen bonding, and solvent interactions.

2.4. Aquatic photochemistry and mechanisms

Complex photochemical reactions between chromophoric dissolved organic matter (CDOM) and contaminants in natural water under solar irradiation play a crucial role in determining the fate of these contaminants. AQ2S has often been used as a surrogate for CDOM compounds in studies involving the phototransformation of various contaminants, such as ibuprofen (IBP), atrazine, nitrite (NO_2^-), and 2-chlorobiphenyl in surface water [79–82]. Unlike some other CDOM compounds, AQ2S is hardly able to directly yield $^{\bullet}OH$ or $^1O_2$ under irradiation [83], making it an ideal tool for determining reaction rate constants (e.g., $k_{^3AQ2S^*,IBP} = 9.70 \times 10^9 \, M^{-1} \, s^{-1}$) [79]. In addition, under ultraviolet A (UVA) irradiation, AQ2S facilitates the oxidation of NO_2^- to $^{\bullet}NO_2$, thereby inducing phenol nitration [81]. The notably higher reduction potential of the triplet excited state of AQ2S ($^3AQ2S^*$, $E° = 2.3$ V_{NHE}, the normal hydrogen electrode) compared to that of the normal triplet excited state of CDOM ($^3CDOM^*$, $E° = 1.3–1.9 \, V_{NHE}$) underscores the heightened reactivity of the former [84–87]. In this case, most $^3CDOM^*$ in the surface water is less oxidizing than $^{\bullet}OH$ [88]. Consequently, $^3AQ2S^*$ represents an upper limit for typical $^3CDOM^*$ reaction rates and may inadequately represent the behavior of natural CDOM [84].

Furthermore, the photochemical reaction of AQs with halide ions is particularly interesting. A defining feature distinguishing seawater from freshwater is its elevated halide concentration [89]. Excited states of AQs can convert halides (e.g., Br^- and Cl^-) into

reactive halogen species, such as $Br_2^{\bullet-}$, $Cl_2^{\bullet-}$, and $ClBr^{\bullet-}$ [33,89–91], significantly affecting the photoconversion of marine organic compounds [89]. Halide ions (X^-) react with $^3AQ^*$ to form charge-transfer binary exciplex intermediates, such as $^3(AQ-X)^{*-}$. As the reduction potential of $Br^{\bullet}$ (1.92 V_{NHE}) is lower than that of $Cl^{\bullet}$ (2.5 V_{NHE}), the Br^- exciplex is formed more easily [36,89]. At halide concentrations below 10 mM, owing to the "heavy-atom effect" of halides, the exciplex primarily undergoes radiationless transitions to the ground state (equation (1)) [87,92]. The quenching effect increases with higher spin-orbit coupling (ζ) in the $X^{\bullet}$ radical according to the order $\zeta(Cl^{\bullet}) < \zeta(Br^{\bullet}) < \zeta(I^{\bullet})$ [92]. $^3(AQ-X)^{*-}$ can also be separated to form a radical pair [87].

$$^3AQ^* + Br^- \rightarrow {}^3(AQ\text{-}Br)^{*-} \rightarrow AQ + Br^- \qquad (1)$$

$$^3AQ^* + Br^- \rightarrow {}^3(AQ\text{-}Br)^{*-} + Cl^- \rightarrow {}^3(AQ\text{-}Br\text{-}Cl)^{*2-} \rightarrow AQ^{\bullet-} + BrCl^{\bullet-} \qquad (2)$$

$$^3AQ^* + Cl^- \rightarrow {}^3(AQ\text{-}Cl)^{*-} + Cl^- \rightarrow {}^3(AQ\text{-}Cl\text{-}Cl)^{*2-} \rightarrow AQ^{\bullet-} + Cl_2^{\bullet-} \qquad (3)$$

Furthermore, the radical yield is highly related to the halide ion concentrations. At halide ion concentrations greater than 0.1 M, the binary complex may react with halide ions to form a ternary complex (e.g., $^3(AQ\text{-}Cl\text{-}Cl)^{*2-}$ and $^3(AQ\text{-}Br\text{-}Cl)^{*2-}$) (equation (2) and (3)). As the nascent dihalide radicals are not involved in the spin-orbital coupling ($\zeta(Cl_2^{\bullet-}) = \zeta(Br_2^{\bullet-}) = \zeta(I_2^{\bullet-}) = 0 \, cm^{-1}$) to the $^3AQ^*$ intersystem crossing, ternary complexes are more likely to separate to produce radical pairs ($X_2^{\bullet-}$ and $AQ^{\bullet-}$) rather than reverting to the ground state via intersystem crossing (equation (2) and (3)) [89,92]. Reactive halogen species generated from ternary complexes prevail because of the low reduction potential of Br^- [89]. Halide ions are abundant in seawater (e.g., 540 mM Cl^- and 0.8 mM Br^-). For halide concentrations greater than 0.1 M, the yield of photosensitizer radical anions correlates directly with halide concentration; for instance, AQ2S in 0.54 M Cl^- yielded a radical yield of approximately 35% [36,87]. Overall, AQs photocatalysts are promising for pollutant removal, particularly in water environments rich in halide ions, such as seawater, reverse osmosis concentrates, and landfill leachate.

3. Environmental application of AQs-based photocatalysis

AQs have garnered increasing interest due to their excellent optical and electron-mediated properties, as well as their low cost, controllable structures, and ease of preparation. They find diverse applications in photochemical processes, such as H_2 production [93], H_2O_2 synthesis [94], organic synthesis [67], pollutant degradation [1], PDT [39], antiviral applications [95], and photocatalytic antibacterial activity [40]. Table 2 summarizes the various applications and roles of AQs in photocatalysis.

3.1. H_2O_2 production

3.1.1. Photocatalytic production of H_2O_2

H_2O_2 is an environmentally friendly oxidant with applications in organic synthesis, wastewater treatment, and disinfection [96]. Industrial H_2O_2 synthesis typically involves the autoxidation of AQs, where 2-ethylanthraquinone undergoes palladium (Pd)-catalyzed hydrogenation to form an AHQ-type structure (Fig. 2a) [97]. Subsequently, AHQ reacts with O_2 to produce H_2O_2. However, challenges arise with using precious metal catalysts, leading to excessive hydrogenation and rapid catalyst deactivation, pollution from organic solvents, and waste generation [96,98].

As described in Section 2, AQs, as photochemically active organic molecules, can be reduced to AHQ in the presence of suitable electron or hydrogen donors. They act as hydrogen carriers

Table 2
The environmental application of AQs-based photocatalyst.

Photocatalyst	Dosage (g L^{-1})	Lamp (W)	Irradiation time (h)	The role of AQs in ROS generation	Efficiency	Reference
2-Ethylanthraquinone	25	Full-spectrum irradiation	4	Generation of H$_2$O$_2$	The maximal H$_2$O$_2$ concentration of 574.0 mM	[99]
g-C$_3$N$_4$/AQ-COOH	0.5	150 W Xenon Arc lamp (simulated solar light)	2	Generation of H$_2$O$_2$	Net H$_2$O$_2$ production rate of 361 μmol g^{-1} h^{-1}	[100]
AQ-COOH/P-doping g-C$_3$N$_4$	5	300 W Xenon lamp (400−780 nm)	3	Enhanced H$_2$O$_2$ production	H$_2$O$_2$ production rate of 75 μM h^{-1}	[38]
AQ-COOH/carbon dots	0.176	150 W Xenon Arc lamp (simulated solar light)	2	Enhanced electron transfer kinetics for H$_2$O$_2$ production	H$_2$O$_2$ production rate of 593.9 μmol g^{-1} h^{-1}	[101]
Nylon fibers loaded with AQ2S	12 × 10 cm^2	400 W UVA lamp 365 nm	0.75	Generation of •OH in the presence of organic hydrogen donors	Completely decolorized 2,6-dichloroindophenol	[76]
AQ2S-polypyrrole-ZnIn$_2$S$_4$	0.3	150 W Halogen cold-visilight-source	3	Promoting ROS production	The tetracycline removal rate exceeded 98%	[102]
AQ2S@rGO	0.1	300 W Xenon lamp (simulated solar light)	2.5	The radical anion of AQ2S generated ROS such as O$_2^{•-}$	99% removal of sulfadiazine in water containing 0.5 M NaCl	[1]
Emodin-hydroxyapatite	0.8	32 W Compact fluorescent lam (400 −780 nm)	0.5	Promoting the production of O$_2^{•-}$	Completely photodisinfection of *Staphylococcus aureus*n	[103]
AQ2S-GO	0.03	3 W LED visible light	2.7	AQ2S enhanced ROS yield	Photo-induced inhibition effect of *Escherichia coli* was 99%	[40]
g-C$_3$N$_4$-AQ-MoO$_3$	1.0	300 W Xe lamp (simulated sunlight)	3	Promoting ROS production	Rate of H$_2$ generation 672 μmol g^{-1} h^{-1}	[93]
AQ-NiTiO$_3$-g-C$_3$N$_4$	1.0	500 W Halogen lamp (visible light)	5	-	Rate of H$_2$ generation 576 μmol g^{-1} h^{-1}	[104]
Perylene-anthraquinone donor-acceptor conjugated microporous polymer	0.28	300 W Xe lamp (visible light)	2	Promoting the production of O$_2^{•-}$	96% photoreduction of U(VI) efficiency at pH = 1	[26]
AQ2S	0.31	200 W White lamp (λ > 400 nm)	24	-	The selectivity of aerobic oxidation of toluene to benzaldehyde was 89.4%	[105]
2,6-diaminoanthraquinone-COF	0.5	12 W LED green light	1.5	O$_2$ reacted with electrons on LUMO, and generated O$_2^{•-}$	The selectivity of primary amines to imines was 99%	[106]

Abbreviations: AQs, anthraquinone and its derivatives. ROS, reactive oxygen species. g-C$_3$N$_4$, graphitic carbon nitride. AQ-COOH, anthraquinone-2-carboxylic acid. AQ2S, anthraquinone-2-sulphonate. •OH, hydroxyl radicals. rGO, reduced graphene oxide. O$_2^{•-}$, superoxide radicals. GO, graphene oxide. AQ, anthraquinone. COF, covalent organic framework. LUMO, lowest unoccupied molecular orbital.
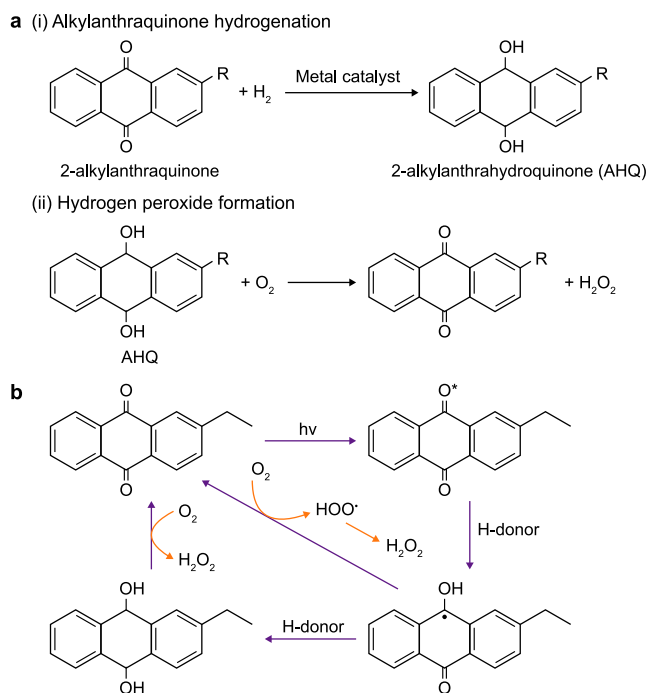
Fig. 2. a, AQs autoxidation process for H$_2$O$_2$ production. Adapted with permission from Ref. [97]. Copyright 2006, Wiley. **b**, Proposed mechanism for photocatalytic H$_2$O$_2$ production over 2-ethylanthraquinone. Adapted with permission from Ref. [99]. Copyright 2016, Elsevier B.V.

by transferring hydrogen to O$_2$ to produce H$_2$O$_2$ [99]. Therefore, synthesizing H$_2$O$_2$ by photoinduced reduction of AQs is an alternative method. For instance, 2-ethylanthraquinone is a water-insoluble organic photosensitizer in photocatalytic H$_2$O$_2$ production [98,99]. As shown in Fig. 2b, in an intermolecular photochemical process, 2-ethylanthraquinone is photoreduced to AHQ by extracting hydrogen from the solvent (water and almost any organic compound) and is subsequently oxidized by O$_2$ to produce H$_2$O$_2$ under Xenon lamp irradiation and air bubbling [98]. Chen et al. [99] demonstrated the optimal production of H$_2$O$_2$ using 1,3,5-trimethylbenzene as the hydrogen donor via 2-ethylanthraquinone catalysis in the aqueous phase.

In addition to their photocatalytic synthesis of H$_2$O$_2$, AQs can enhance the semiconductor photocatalytic production of H$_2$O$_2$. g-C$_3$N$_4$ is considered a promising metal-free photocatalyst; however, it exhibits limited visible light absorption capacity, and the photogenerated e$^-$ and h$^+$ easily recombine. To enhance photocatalytic H$_2$O$_2$ formation, anchoring AQs to g-C$_3$N$_4$ represents a promising approach [38,94,100,107]. For instance, anchoring AQ-COOH to g-C$_3$N$_4$ improves carrier separation, with AQ-COOH accepting electrons in the CB of g-C$_3$N$_4$ and undergoing electron-coupled hydrogenation reactions (AQ → AHQ). Subsequently, AHQ is dehydrogenated to revert to AQ, while O$_2$ is reduced to H$_2$O$_2$ [100]. Kim et al. [100] employed a heat-induced hybridization process to prepare AQ-COOH-augmented g-C$_3$N$_4$, establishing linkages via amide bonds and π−π interactions. Upon coupling with AQ-COOH, the hybrid material showed a decrease in intensity and a shift toward higher energies of the C=O peak (531.4 eV) and −COOH peak (533.2 eV) compared to those of AQ-COOH, indicating the successful incorporation of AQ-COOH. This incorporation was

confirmed by X-ray photoelectron spectroscopy of the amide bond ($O=C-N$, 532.4 eV) (Fig. 3a) [100]. The linear sweep voltammetry curves of g-C_3N_4/AQ-COOH (Fig. 3b) demonstrated a positively shifted reduction peak potential and an increased reduction current under oxygen-saturated conditions compared with that of g-C_3N_4, indicating that AQ-COOH enhanced the oxygen reduction process [100]. Furthermore, the H_2O_2 production rate over g-C_3N_4/AQ-COOH reaches 361 μmol g^{-1} h^{-1} when isopropanol serves as the organic electron donor, with a more pronounced cocatalytic effect of AQ-COOH observed in the absence of a sacrificial electron donor [100]. Similarly, Ye et al. [38] conducted P doping and edge modification of ultrathin g-C_3N_4 nanosheets, loading AQ-COOH onto the g-C_3N_4 surface via $\pi-\pi$ interaction. Fourier transform infrared spectra of AQ-COOH-modified g-C_3N_4 (Fig. 3c) exhibited characteristic peaks for −COOH and −C=O groups in AQ-COOH. This hybrid material demonstrated superior H_2O_2 generation compared to its counterparts under visible light irradiation (Fig. 3d). Chu et al. [107] confirmed the selective anchoring of AQ-COOH through the photoreduction of noble metals on the edges of g-C_3N_4 [107].

Carbon dot (CD)-based photocatalysts with strong optical absorption and controlled functional groups, such as hydroquinone, hydroxyl, and carboxyl groups, have shown promise in H_2O_2 evolution [101,108]. In the presence of ethanol as an electron donor, CD exhibited a high H_2O_2 generation rate (631.8 μmol g^{-1} h^{-1}) [101]. Remarkably, even without ethanol, the material demonstrated excellent photocatalytic performance for H_2O_2 production, reaching 609.4 μmol g^{-1} h^{-1} under the same conditions, surpassing g-C_3N_4. Introducing AQ-COOH onto the CD surface (CD-AQ) by forming amide bonds enhances photocatalytic performance by reducing photogenerated e$^-$−h$^+$ recombination and favoring the two-electron pathway of the oxygen reduction reaction (ORR) [101]. The H_2O_2 yield of CD-AQ under simulated solar illumination for 2 h surpassed that of bare CD or a physical mixture of CD and

AQ-COOH (Fig. 3e). Since photocatalytic H_2O_2 production is governed by the proton-coupled electron transfer (PCET) reaction ($O_2 + 2H^+ + 2e^- \rightarrow H_2O_2$), the CD-AQ photocatalytic production of H_2O_2 was strongly influenced by pH. Based on experimental results and theoretical calculations, the proposed mechanism (Fig. 3f) of CD-AQ photocatalytic H_2O_2 generation involves photoexcited CD transferring electrons to AQ, which promotes carrier separation, while AQ-COOH undergoes a hydrogenation/dehydrogenation reaction to selectively generate H_2O_2. Photogenerated h$^+$ oxidizes ethanol to CO_2, in the absence of ethanol, h$^+$ oxidizes the −OH groups on the CD surface to carbonyl groups or H_2O to O_2. Protons required in the PCET reaction can be supplied by −COOH on the CD surface or generated by −OH when electron and proton donors are absent [101].

3.1.2. Photoelectrochemical production of H_2O_2

AQ-modified electrodes are utilized as cathodes in electrochemical and photoelectrochemical systems for ORR [109,110]. Jeon et al. [109] synthesized AQ-modified single-walled carbon nanotube (CNT) cathodes (AQ-CNT/C) via a drop-casting method, exhibiting reduced charge transfer resistance compared to an unmodified CNT cathode. Moreover, the presence of O_2 further reduced the charge transfer resistance, indicating that AQ promoted the intramolecular electron transfer and exhibited high selectivity for H_2O_2 production via the ORR instead of the water reduction reaction [109]. In summary, AQs play versatile roles in the photocatalytic synthesis of H_2O_2 applications, both in catalyzing the photosynthesis of H_2O_2 alone and in enhancing H_2O_2 production in semiconductor photocatalytic/photoelectrocatalytic systems to address environmental and industrial challenges.
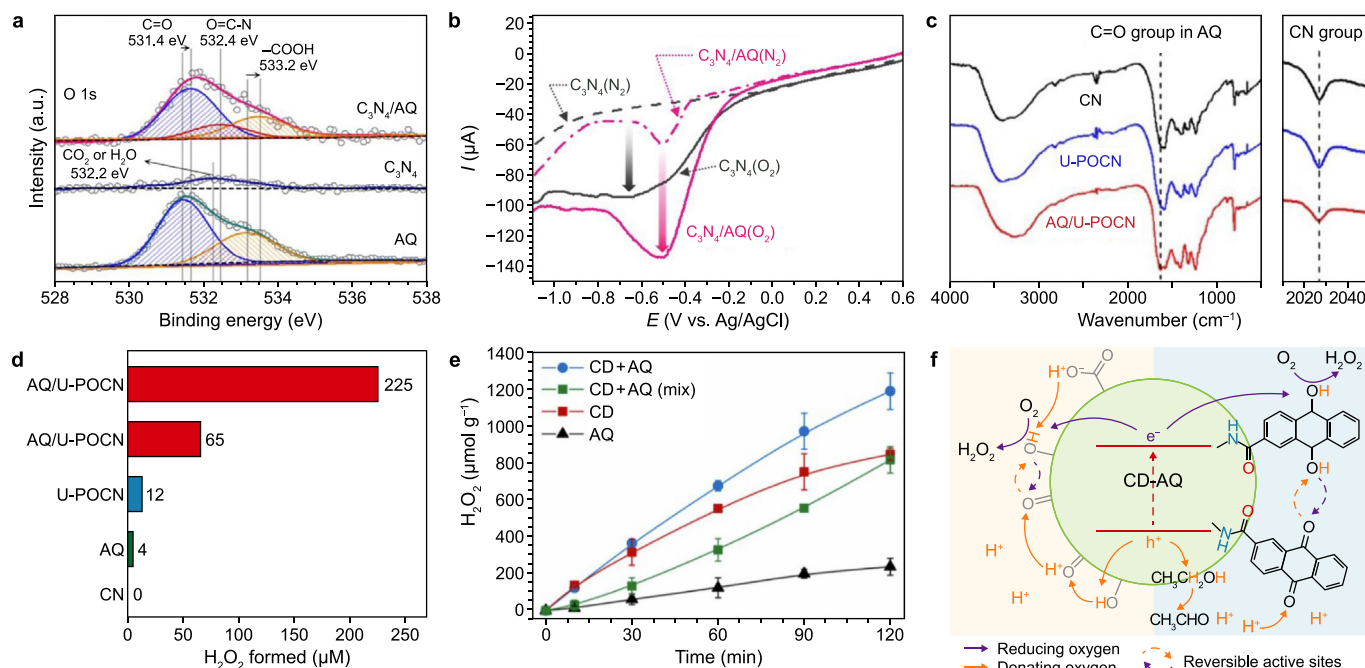
Fig. 3. a, High-resolution O 1s X-ray photoelectron spectra of on AQ-COOH, g-C_3N_4, and g-C_3N_4/AQ-COOH. **b**, linear sweep voltammetry curves of g-C_3N_4 and g-C_3N_4/AQ-COOH (10 wt%). Adapted with permission from Ref. [100]. Copyright 2018, Elsevier B.V. **c**, Fourier transform infrared spectra of CN, U−POCN, and AQ/U−POCN. **d**, Amounts of H_2O_2 generated within 3 h by visible photocatalysis by CN, U−POCN, and AQ/U−POCN. Adapted with permission from Ref. [38]. Copyright 2020, Elsevier B.V. **e**, Time curves of H_2O_2 production under visible light irradiation by CD, AQ-COOH, CD-AQ, and a physical mixture of CD and AQ; **f**, Proposed mechanism for photocatalytic H_2O_2 production over CD-AQ. Adapted with permission from Ref. [101]. Copyright 2022, Elsevier B.V.

3.2. H_2 evolution

The photocatalytic decomposition of water for H_2 production offers significant benefits, including low cost, high performance, and green chemistry, making it a subject of keen interest among researchers tackling energy challenges [8]. Commonly used catalysts include photosensitizers and semiconductors containing metal oxides, metal sulfides, and g-C_3N_4 [111–113]. Despite considerable progress in photocatalyst development, many catalysts still require improvement due to low quantum efficiency, rapid recombination of photogenerated carriers, and underutilization of solar light. In composite photocatalytic systems, AQ can act as an electron transfer channel, being reduced to AHQ by e^- in the CB of one semiconductor and then oxidized back to AQ by h^+ in the VB of another semiconductor. AQ facilitates the efficient separation and migration of photogenerated e^- and h^+ [93,114]. Ma et al. [93] developed a ternary Z-scheme g-C_3N_4-AQ-MoO_3 photocatalytic system for efficient H_2 production, with a transmission electron microscope image confirming the presence of the three components in the hybrid composite (Fig. 4a) [93]. The ternary Z-scheme structure of g-C_3N_4-AQ-MoO_3 is illustrated in Fig. 4b. Based on the characterization results, the authors proposed that AQ molecules are attached to the surface of MoO_3 nanorods and covered by the g-C_3N_4 nanosheets. The addition of AQ enhances the separation of photogenerated carriers and the charge transfer capability of ternary g-C_3N_4-AQ-MoO_3 compared to other materials, as evidenced by transient photocurrent response spectra, photoluminescence spectra, and electrochemical impedance spectroscopy (Fig. 4c–e). Similarly, a Z-scheme heterojunction $NiGa_2O_4$-AQ-MoO_3 was employed for the simultaneous light-driven conversion of nitrite and sulfite [114]. Fig. 4f depicts the possible electron transfer pathways of the ternary composite under solar irradiation, with triethanolamine acting as a scavenger for h^+ in MoO_3. AQ is reduced by e^- from the CB of MoO_3 to form AHQ, and h^+ from the VB of g-C_3N_4 oxidizes AHQ back to AQ.

1,5-Diamino-4,8-dihydroxyanthraquinone (DAHA) exhibits strong absorption in the red part of the solar spectrum, with a peak at 614 nm (Fig. 4g) [115]. In a photocatalytic H_2 production system designed by Ming et al. [115], DAHA was employed as a light-absorbing component. Co(dmgH)$_2$(py)Cl (dmgH = dimethylglyoxime, py = pyridine) served as the molecular catalyst for proton reduction, with the dimethylglyoxime ligand stabilizing the cobalt catalyst. Ammonium bromide and 1,3-dimethyl-2-phenyl-2,3-dihydro-1*H*-benzo[*d*]imidazole acted as proton and electron donors, respectively [115]. The rate of H_2 production was positively correlated with the concentration of DAHA under red light irradiation (Fig. 4h). Light also controlled the switch for H_2 production (Fig. 4i) [115]. Inspired by natural photosynthesis, Li et al. [116] reported a metal-organic tetrahedron modified with 2,6-diaminoanthraquinone (DAAQ). The electron-deficient DAAQ acts as an electron shuttle, with encapsulated fluorescein organic dye enabling light-induced H_2 production from water. In summary, during photocatalytic H_2 production, AQs primarily act as light-absorbing components and redox mediators to accelerate the migration of photogenerated carriers. Designing visible-light-responsive photoactive materials grafted with AQs represents a promising strategy for efficient photocatalytic H_2 production.

## 3.3. Degradation of pollutants

Photocatalysis has garnered significant research attention worldwide due to its ability to generate potential oxidizing radicals and exhibit rapid reaction rates. Solar-driven photocatalysis is particularly effective in degrading harmful organic pollutants into harmless inorganic small molecules, such as H_2O and CO_2, achieving high mineralization rates and minimizing the release of deleterious byproducts, thereby facilitating environmental remediation [117,118]. In a study by Sun et al. [76], AQ2S was immobilized on nylon (polyamide) fibers using an acid-dyeing process, resulting in the photoactive self-cleaning properties of the dyed nylon. This dyed nylon effectively catalyzed the degradation of 2,6-dichloroindophenol (DCIP) under UVA irradiation [76]. Although both the original nylon fabric and the dyed nylon exhibited excellent decolorization effects on DCIP, the original nylon fabric only functioned as an adsorbent, whereas the color of DCIP in the AQ2S dyed fiber gradually disappeared. Upon exposure to UVA irradiation, the AQ2S in the dyed fibers transformed into a triplet excited state, readily abstracting hydrogen atoms from nylon with weaker N−H bonds to produce an AQ2S radical. The triplet radicals of AQ2S then interacted with O_2 to produce $^\bullet OH$ and ROS, facilitating the oxidation of DCIP. Moreover, under UVA irradiation, AQ2S achieved complete decolorization of a textile colorant (reactive black 5) within 10 min with the addition of hydrogen donors (e.g., isopropanol and dimethyl sulfoxide) to aqueous solutions [68]. These hydrogen donors transferred H-atoms or electrons to $^3AQ^*$, with O_2 being essential for ROS generation ($^\bullet OH$, $O_2^{\bullet-}$, and H_2O_2) crucial for removing reactive black 5 [119].

Given their redox-active groups featuring quinone/hydroquinone structures, AQs can function as electron shuttles to facilitate the biodegradation of pollutants and biogeochemical cycling [120,121]. For instance, anthraquinone-2,6-disulfonate (AQDS) facilitates electron transfer during microbial Fe(III) reduction [121]. In addition to their redox properties, AQs' photosensitivity can be harnessed to construct extracellular photoelectron storage carriers that link photochemical and microbial reactions to achieve solar-to-chemical conversion [120]. Chen et al. [120] implemented an AQ2S-based semiartificial photosynthetic system for microbial denitrification. In this system, AQ2S assumed the dual roles of a microbial photosensitizer and an electron capacitor. Under light irradiation (Fig. 5a), the photochemically active AQ2S formed $^3AQ2S^*$, which underwent electron transfer from lactate molecules (electron donors) to produce AQ2S$^{\bullet-}$. This AQ2S$^{\bullet-}$ then transferred electrons to *Thiobacillus denitrificans* (*T. denitrificans*, an autotrophic nonphototrophic denitrifier) through extracellular electron acceptors. Under dark conditions, AQ2S$^{\bullet-}$ transitioned to a reduced state (H-AQ2S) via proton transfer, with H-AQ2S acting as an extracellular capacitor to capture unused electrons and release stored electrons to *T. denitrificans*. After 10 h of irradiation, NO_3^-−N was completely removed in the presence of *T. denitrificans* and AQ2S, as illustrated in Fig. 5b. Increasing the concentration of AQ2S and prolonging the light duration enhanced nitrous oxide (N_2O) production. It is important to note that considering the solubility of AQ2S, AQ2S-contaminated wastewater may be generated during NO_3^-−N reduction. Therefore, further efforts are needed to develop technologies for immobilizing AQS on solid-phase substrates.

As discussed in Section 2.4, the photochemical interactions of $^3AQs^*$ with halide ions in water containing halide ions can generate halogen radicals, which are important for pollutant degradation [1,16]. Halogen radicals attack organic substrates through hydrogen abstraction, halogen addition, and electron abstraction (Fig. 5c). These radicals undergo hydrogen abstraction reactions with saturated aliphatic compounds [87]. The reaction of $Cl^\bullet$ is generally fast ($k = 10^7–10^9$ M^{-1} s^{-1}), whereas other halogen radicals ($Br^\bullet$ and $Cl_2^{\bullet-}$) react more slowly [122,123]. Halogen radicals also attack olefinic substances through addition reactions, forming halogenated products [122]. For aromatic compounds, $Cl_2^{\bullet-}$ undergoes addition reactions with substrates bearing electron-withdrawing groups ($k < 10^5–10^7$ M^{-1} s^{-1}), while electron abstraction reactions with substrates carrying electron-donating groups ($k = 10^7–10^9$ M^{-1} s^{-1}) are preferred [122]. Considering the
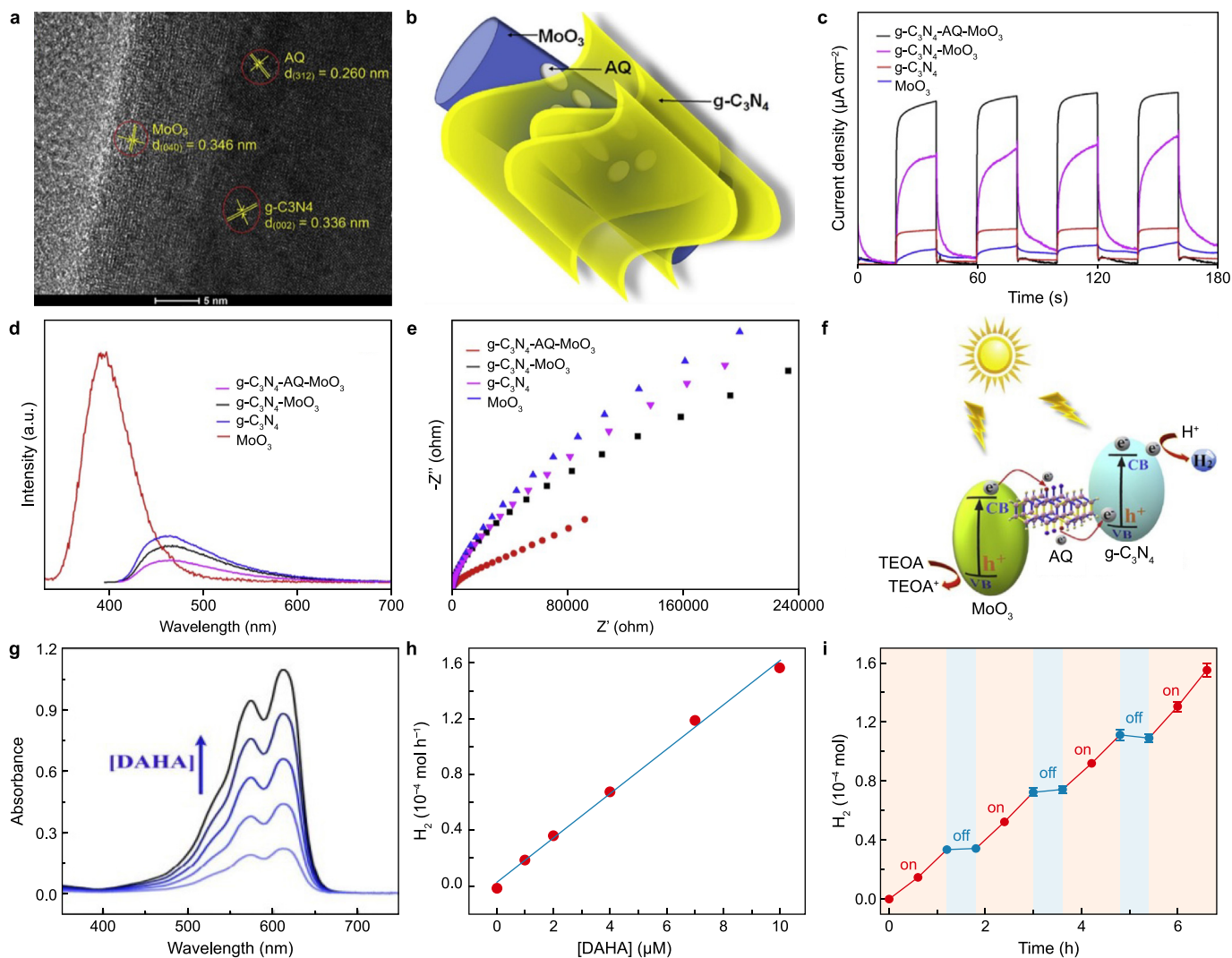
Fig. 4. a, The transmission electron microscope image of g-C₃N₄-AQ-MoO₃ composite. **b**, schematic illustration for the structure of Z-scheme g-C₃N₄-AQ-MoO₃. **c−e**, photoluminescence spectra (**c**), transient photocurrent response spectra (**d**), and electrochemical impedance spectra (**e**) of g-C₃N₄, MoO₃, g-C₃N₄-MoO₃, and g-C₃N₄-AQ-MoO₃ composite. **f**, Possible mechanism of photocatalytic hydrogen production over g-C₃N₄-AQ-MoO₃ under simulated sunlight irradiation. Adapted with permission from Ref. [93]. Copyright 2021, Elsevier B.V. **g**, UV−vis absorption spectra of different concentrations of DAHA. **h**, Plot of the rate of H₂ production versus [DAHA] concentration. **i**, H₂ production at an initial [DAHA] of 2 μM with lights on and lights off. Adapted with permission from Ref. [115]. Copyright 2022, American Chemical Society.

interaction between photosensitive AQs and halide ions under suitable light irradiation and the potential for AQs to contaminate effluents, our research group prepared a series of composites using graphene as a substrate material, which is rich in reactive sites and exhibits superior electron transfer properties [1,16,124]. The catalytic degradation behavior and mechanism of sulfadiazine and trimethoprim by the photocatalytic composites were investigated in aqueous solutions containing high concentrations of Cl⁻ under solar irradiation. $Cl_2^{\bullet-}$ and ROS were the main reactive radicals. The reaction system efficiently degraded various micropollutants in a 0.5 M NaCl aqueous solution under 40 min of simulated sunlight irradiation (Fig. 5d). A sufficient concentration of Cl⁻ in a water body is crucial for removing organic pollutants using this photocatalytic system. AQs play an essential role in the photocatalytic degradation of pollutants, suggesting that AQs-based photocatalytic systems hold promise for treating contaminated water, especially in Cl⁻-containing environments.

3.4. Antibacterial application

The misuse of antibiotics has resulted in severe bacterial resistance, notably giving rise to "super bacteria". In recent years, nanoantibacterial materials have emerged as effective solutions to overcome bacterial drug resistance [40]. The photoinduced antibacterial function of AQs is primarily attributed to ROS. Cotton-based medical and functional textiles and cellulose nanocrystals are often loaded with AQs by π−π interactions and covalent binding to eliminate microorganisms [77,78,125−127]. For instance, Liu et al. [77] loaded AQ-COOH onto cotton fibers to synthesize cotton fabrics with self-cleaning and sterile properties, achieving over 99% inactivation of *Escherichia coli* (*E. coli*) and *Staphylococcus aureus* (*S. aureus*) under UVA irradiation. Cardoso et al. [125] prepared a low-cost covalently linked AQ-cotton fabric with visible light responsiveness, achieving 99.9% inhibition of *E. coli* due to the generation of highly reactive ¹O₂. Furthermore, reactive blue P-3R, an AQ derivative and photoactive compound, can be incorporated into polyamide 56 fabrics via covalent bonding, demonstrating
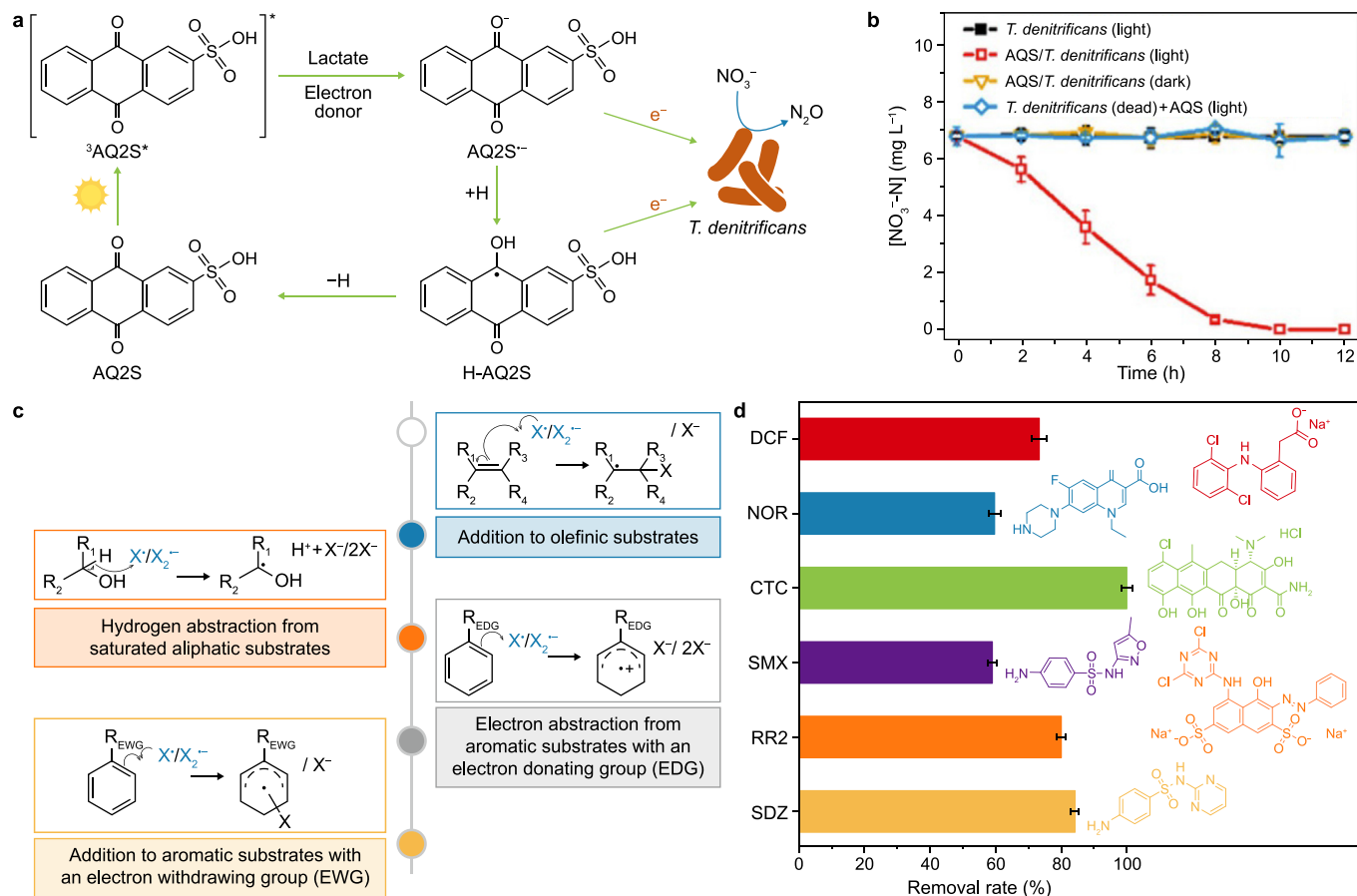
Fig. 5. a, Proposed mechanism for N₂O production by AQ2S/*Thiobacillus denitrificans*. **b**, Time-dependent profiles of nitrate reduction by AQ2S/*T. denitrificans*. Adapted with permission from Ref. [120]. Copyright 2022, American Chemical Society. **c**, Proposed mechanisms for the reaction of halogen radicals (X�• and X₂•⁻) with organic substrates. Adapted with permission from Ref. [87]. Copyright 2018, American Chemical Society. **d**, The removal effects of AQC/AGR on different organic pollutants (DCF, diclofenac; NOR, norfloxacin; R CTC, chlortetracycline hydrochloride; SMX, sulfamethoxazole; R2, reactive red 2; SDZ, sulfadiazine). Adapted with permission from Ref. [16]. Copyright 2023, Elsevier B.V.

good antimicrobial effects against *E. coli* and *S. aureus* [78]. These AQ-modified materials are promising for medical textiles and bio-materials [78]. Further, AQ-COOH-functionalized cellulose nano-crystals with hydrophilicity and superior photoinduced antibacterial and self-cleaning properties are expected to be applied in protective clothing [127].

Graphene oxide (GO) is a graphene derivative with a two-dimensional (2D) structure with a high specific surface area, abundant oxygen-containing functional groups, and good biocompatibility. GO is a good choice as a carrier for AQs and is used as a photocatalytic antibacterial agent. Zhang et al. [40] combined AQ2S with GO through π–π interactions to create AQ2S-GO nanocomposites, which exhibited potent antibacterial activity for the photoinduced inactivation of *E. coli*, effectively inhibiting its growth. Bacterial cells treated with the AQ2S-GO composite exhibited complete distortion within 160 min of visible light irra-diation, whereas materials treated in the dark showed relatively poor antibacterial properties. As illustrated in Fig. 6a, when initially rod-shaped *E. coli* cells with intact cell membranes (0 min) were exposed to visible light irradiation, the reactive species produced by AQ2S-GO destroyed the outer cell membrane. They formed small pores on the bacterial surface, resulting in cell death (160 min) [40]. Furthermore, the photic bactericidal effect of AQ2S-GO was significantly greater than that of GO at the same concentration, with the proportion of *E. coli* cell survival decreasing to 0.01 for AQ2S-GO compared to 0.77 for GO. The formation of a Z-scheme

heterojunction between AQ2S and GO generated •OH and O₂•⁻, thereby enhancing antibacterial efficiency (Fig. 6b).

Emodin (1,3,8-trihydroxy-6-methylanthraquinone) is a low-toxicity herbal medicine with antibacterial, antiviral, and anti-fungal properties that has been widely used since ancient times. It is extracted from the roots and stems of several medicinal plants via phytoextraction [103]. Emodin exhibits antimicrobial activity un-der dark conditions and displays stronger antibacterial activity under visible light conditions, acting as a photosensitizer to pro-duce ROS [103]. The combination of emodin and hydroxyapatite (HAp) (Emodin/HAp) effectively enhanced the migration of pho-togenerated carriers, facilitating the degradation of tetracycline and inhibiting the pathogenic bacterium *S. aureus* growth [103]. The most significant photocatalytic antibacterial effect against *S. aureus* was observed with Emodin/HAp compared to HAp or emodin alone (Fig. 6c). Combined with band structure analysis, h⁺ and O₂•⁻ were identified as the main reactive species responsible for the photo-catalytic antibacterial activity (Fig. 6d). In summary, AQs-loaded solid-phase matrices or medical textiles exhibit photocatalytic antibacterial and self-cleaning properties, presenting significant potential for photocatalytic antibacterial applications.

3.5. PDT in medicine

PDT represents an innovative approach to treating growth-related malignancies and infections by leveraging the cytotoxic
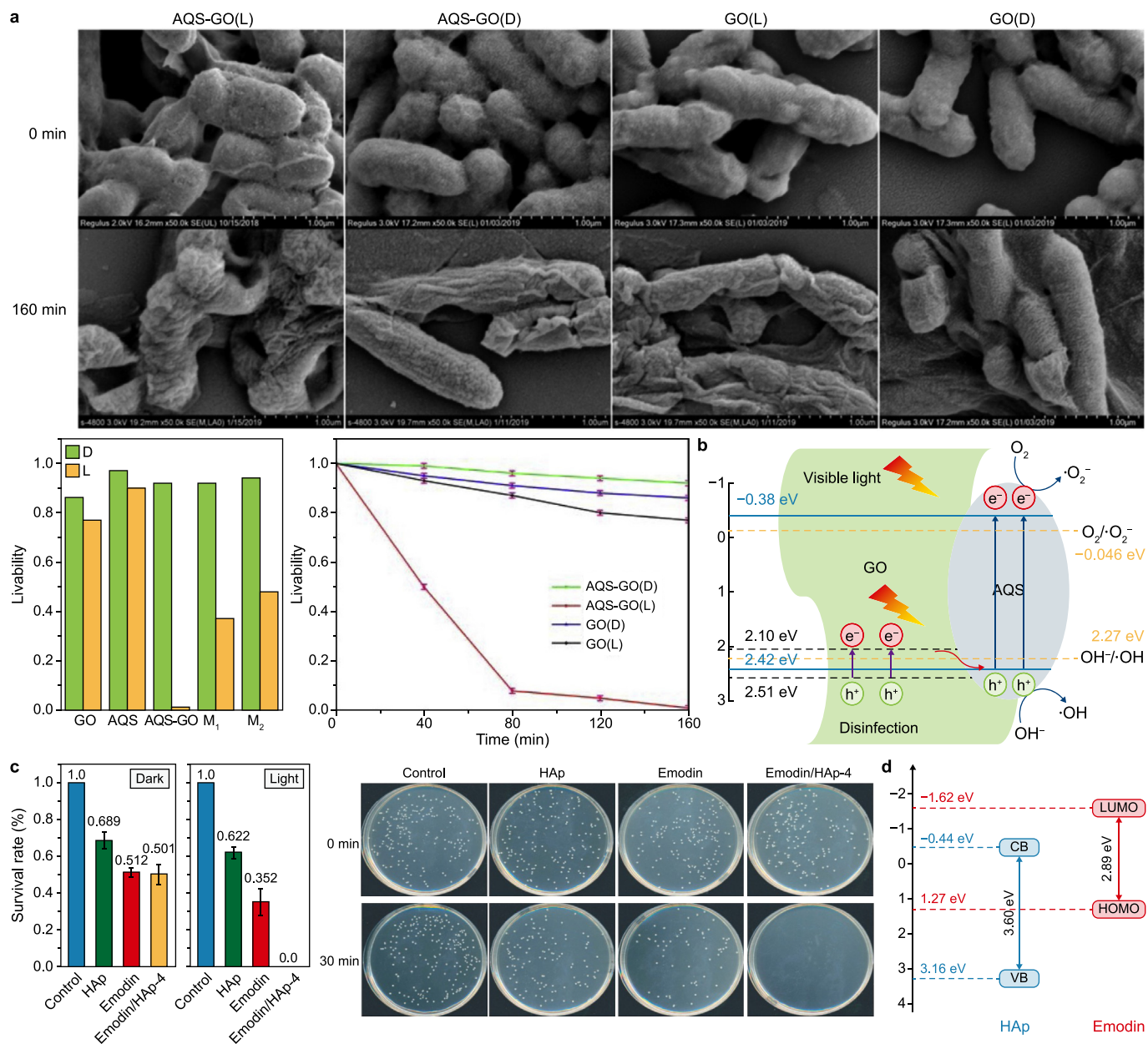
Fig. 6. a, Scanning electron microscopy images and cell viability of *Escherichia coli* treated by GO and AQ2S-GO. **b**, Schematic diagram of ROS generation by AQ2S-GO under visible light. Adapted with permission from Ref. [40]. Copyright 2019, Elsevier B.V. **c**, Survival rates of *Staphylococcus aureus* by the HAp, emodin, and Emodin/HAp-4 photocatalysts. **d**, The band structure of Hap and Emodin. Adapted with permission from Ref. [103]. Copyright 2022, Elsevier B.V.

effects of ROS, such as $O_2^{\bullet-}$ and $^1O_2$ [128,129]. Successful PDT relies on the availability of suitable photosensitizers, oxygen, and specific light wavelengths. AQs demonstrate unique anticancer capabilities, primarily through mechanisms involving deoxyribonucleic acid (DNA) damage, cell cycle arrest, apoptosis, paraptosis, and other effects [130,131]. AQs induce DNA damage by disrupting the double helix structure, thereby inhibiting DNA replication or suppressing DNA topoisomerase activity, resulting in DNA double-strand breaks and inhibition of protein tyrosine kinases [132]. Among AQs, mitoxantrone has demonstrated photosensitizing anticancer effects in human breast cancer cell lines [133]. Certain natural AQs, including lycionine, soranjidiol, bisoranjidiol, 5-chlorosoranjidiol, and 7-chlorobisoranjidiol, exhibit antiparasitic activity against cutaneous leishmaniasis without toxicity to fibroblasts under violet-blue LED irradiation [129]. In one study, de Souza Oliveira

et al. [39] covalently attached amino-functionalized SiO₂ nanoparticles to AQ-COOH and applied this material in PDT for treating A549 lung cancer cell lines, achieving a significant reduction in the cell survival rate (20–30%) after a 15-min treatment period. Sokkar et al. [128] investigated nine commercially available AQs to assess their ability to catalyze ROS production. Energy and electron transfer pathways within AQs that contribute to generating $^1O_2$ and $O_2^{\bullet-}$ were presented. DFT calculations revealed a correlation between the yield $^1O_2$ and the energy gap between the excited singlet state (S1) and the triplet state (T1), with 1,5-diaminoanthraquinone exhibiting the highest $^1O_2$ quantum yield of 0.21. This study highlighted the potential of 1,5-diaminoanthraquinone for PDT applications, and the correlation between the S1-T1 energy gap and the yield of $^1O_2$ can be used to screen and design novel AQs for PDT.

Considering human health risks, it is essential to understand the

structure—activity relationship of AQs, which exhibit varied properties depending on the type and position of substituent groups on the AQ structure. Whereas some AQs demonstrate no toxic side effects under appropriate administration [134], rhein is a potentially hepatotoxic substance. Therefore, establishing toxicological databases and preemptive safety assessments are recommended before the clinical use of AQs in human medicine [135].

3.6. Applications in other fields

3.6.1. Organic synthesis

AQs have versatile applications in organic synthesis, including the selective oxidation of organic sulfides [136] and the aerobic oxidative cyanation of tertiary amines [137]. AQs can catalyze hydrocarbon conversions through site-selective C—H pyridylation via hydrogen atom transfer (HAT) [138], enantioselective radical trifluoromethylation, and aerobic oxygenation of C—H bonds [67,139]. They also catalyze the arylation and alkenylation of aldehydes [140]. AQs demonstrate remarkable photocatalytic abilities in the selective oxidation of p-xylene to p-toluic acid using O_2 or air [25]. The presence of different functional groups (electron-donating and electron-withdrawing moieties) on the aromatic skeleton influences the optical absorption and photocatalytic performance of AQs. For instance, visible light-induced AQ-COOH exhibits a 70.9% conversion of p-xylene, with a highly selective conversion to p-toluic acid reaching 88.2% after 12 h at an O_2 pressure of 1 atm [25]. The generation of benzyl radicals via HAT and PCET (main pathway) mechanisms enables the conversion of benzyl radicals to oxidation products with the participation of O_2 or ROS (Fig. 7a) [25]. Visible light-induced AQ-COOH can catalyze the trifluoromethylation of arenes and heteroarenes by CF_3SO_2Na [141]. In another research area, Bardagi et al. [142] reported the dehalogenation of aryl halides

and the generation of aryl radicals using 1,8-dihydroxyanthraquinone under visible light irradiation. Specifically, 1,8-dihydroxyanthraquinone formed radical and semiquinone anions under a nitrogen atmosphere, with triethylamine as the electron donor and hydrogen donor under photoirradiation, enabling electron transfer to aryl halide. The resulting aryl halide anion was then cleaved into a halide anion and an aryl radical for subsequent formation of C—C bonds [142].

Notably, in sulfonate-substituted AQs, AQDS finds utility in the molecular photoelectrochemistry of benzylic $C(sp^3)$—H bonds for asymmetric catalysis, where highly regioselective C—H breakage occurs, forming benzylic radical intermediates [143]. Excited AQDS and benzylic $C(sp^3)$—H bonds generate ionic radical species during electron transfer, which can further separate into benzylic radicals and semiquinone radical (AQDS—H)$^\bullet$ via proton transfer [143]. The electron-withdrawing —SO_3^- groups of AQDS enhance the reduction potential of AQDS*, influencing the reaction process towards electron/proton transfer rather than HAT [143,144]. AQ2S has also emerged as a promising organophotocatalyst capable of driving the selective oxidation of alcohols to aldehydes and ketones under aerobic conditions and peroxygenase-catalyzed oxy-functionalization reactions [105,145]. The uniform dissolution of AQ2S in the reaction medium eliminates diffusion limitations associated with heterogeneous photocatalysts, thus alleviating the problem of slow reaction kinetics [145].

In addition to homogeneous photocatalysis, AQs have been extensively investigated for their applications in heterogeneous photocatalytic organic synthesis. Li et al. [146] developed a DAAQ-functionalized COF (AQ-COF) linked by β-ketoenamines for visible light-induced selective oxidation of sulfides to sulfoxides. This metal-free photocatalyst exhibits a unique morphology, π-conjugated structure, and high conductivity conductive to efficient
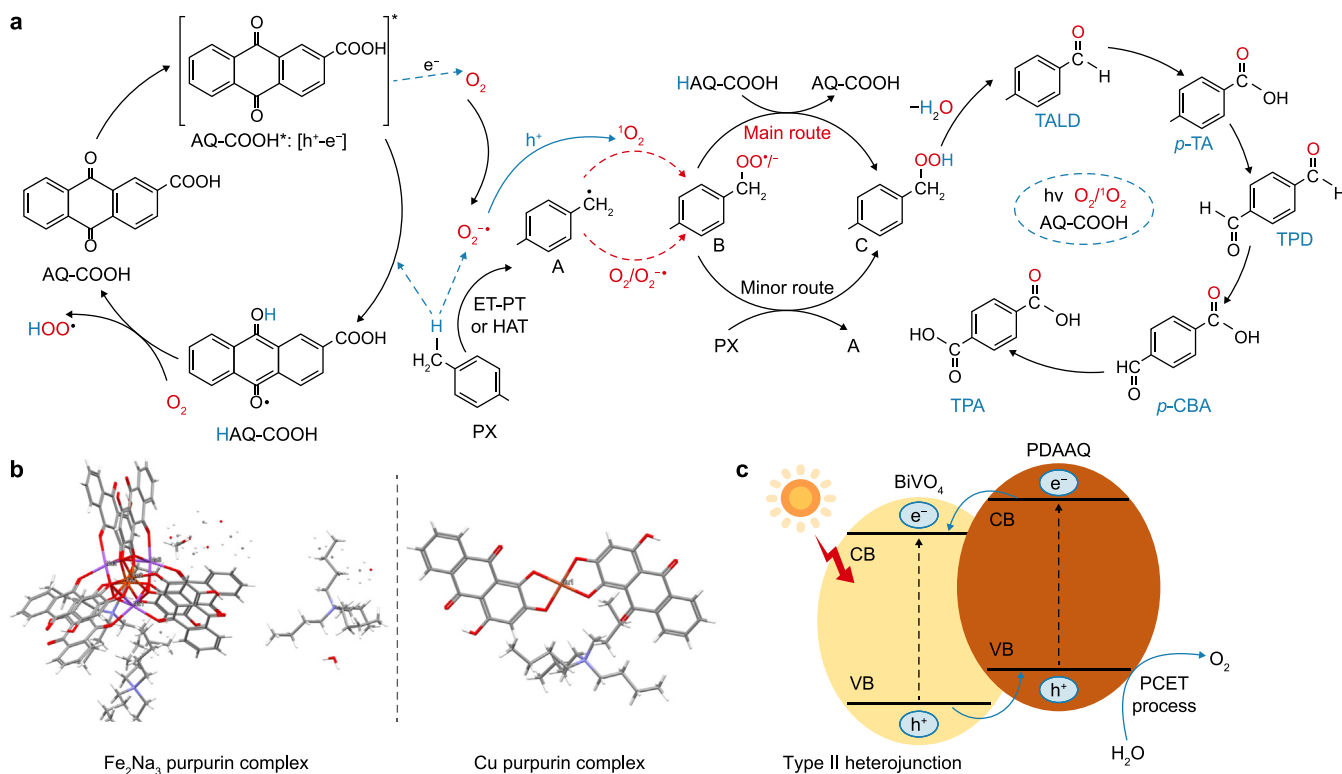
Fig. 7. a, Schematic diagram of p-xylene oxidation by AQ-COOH under visible light. Adapted with permission from Ref. [25]. Copyright 2021, Elsevier B.V. **b**, Crystal structure of Fe purpurin and Cu complex. Adapted with permission from Ref. [148]. Copyright 2022, American Chemical Society. **c**, The photogenerated charge transfer process between PDAAQ and BiVO$_4$. Adapted with permission from Ref. [149]. Copyright 2022, Elsevier B.V.

photogenerated carrier separation. To prevent the dimerization of reduced AQ and enhance catalytic efficiency in photocatalytic HAT reactions, Wang et al. [147] designed a MOF material that encapsulates AQ within Sr-1,4,5,8-naphthalenediimide channels. This innovative approach facilitates rapid electron transfer from reduced AQ to naphthalenediimide, preventing the dimerization of reduced AQ and enhancing the efficiency of the photoacetalization reaction. These studies collectively demonstrate the substantial potential of AQs in both homogeneous and heterogeneous photocatalytic organic synthesis.

3.6.2. Reduction of carbon dioxide

The photocatalytic reduction of CO_2 to produce value-added chemicals represents a promising approach to mitigating the environmental challenges associated with the CO_2-based greenhouse effect and remains attractive [150]. However, low charge separation efficiency and poor product selectivity hinder conventional solar-to-chemical conversion using bare semiconductors. By contrast, organic D–A polymers incorporating polycyclic arenes and AQ have emerged as promising photocatalysts, with AQ serving as an electron mediator that facilitates spatial carrier transport within the polymer matrix. For instance, a polymer comprising AQ and triphenylamine achieves a CO_2 to CO conversion rate of 69.7 μmol g^{-1} h^{-1}, with a remarkable CO selectivity close to 100% under visible-light irradiation [151]. Notably, purpurin (PP), an AQ-based dye derived from madder, exhibits visible-light-driven CO_2 reduction activity when employed as a photosensitizer [148,152,153]. PP acts as a light-harvesting unit and can coordinate with redox-active metals, such as Cu-PP and Fe-PP, facilitating the transfer of excited electrons to these metals for efficient photocatalytic CO_2 reduction (Fig. 7b) [148,153]. Moreover, the stability of photocatalytic materials is a critical consideration in CO_2 reduction applications due to the potential adsorption of competing substances on catalyst surfaces, which can diminish active site availability and overall performance [154].

3.6.3. Oxygen evolution reaction

The electrolysis/photoelectrochemical decomposition of water stands as a promising technology for H_2 production; however, a significant limitation remains the slow four-electron transfer kinetics of the oxygen evolution reaction (OER) occurring at the anode surface [149]. PCET processes can enhance the OER performance of metal-based catalysts by modulating their proton transport properties [149,155]. The carbonyl groups within the AQ structure, known for their exceptional redox activity, serve as effective proton acceptors. Introducing AQs into the photoelectrochemical process may present a potential strategy for enhancing OER activity. An et al. [149] utilized a one-pot method to coat poly-2,6-diaminoanthraquinone (PDAAQ) and γ-Fe$_2$O$_3$ on BiVO$_4$ photoanodes (γ-Fe$_2$O$_3$-PDAAQ@BiVO$_4$). DFT calculations revealed that the VB position of PDAAQ was 0.9 eV higher than that of BiVO$_4$. PDAAQ forms a typical type II heterojunction with BiVO$_4$, enabling the thermodynamically feasible transfer of h$^+$ photogenerated in BiVO$_4$ to PDAAQ (Fig. 7c). This process ultimately promotes the effective separation of photogenerated e$^-$ and h$^+$. Furthermore, the redox activity of PDAAQ accelerates the PCET process of the photoanode, leading to a significant enhancement in its OER activity.

3.6.4. Three-dimensional photo-printing

As previously mentioned, AQs exhibit photochemical activity and redox capacity, making them suitable candidates for forming supramolecular nanostructures via charge-transfer complexes. These complexes hold promise for applications in advanced technologies, such as three-dimensional (3D) printing. Zhang et al.

[156] employed a photochemical approach to modify γ-cyclodextrin (γ-CD) with AQs for the 3D photoprinting of soft materials. In aqueous solution, AQs and γ-CD can form supramolecular quinhydrone charge-transfer complexes in situ under light irradiation. These complexes exhibit high binding affinities, and their nanostructures demonstrate highly stereoselective stacking. γ-CD and AQs were separately polymerized with acrylamide and then subjected to photoprinting under light irradiation in aqueous solutions [156]. Supramolecular photochemistry is capable of selectively modifying materials and is anticipated to be utilized in the design and synthesis of photocatalysts.

3.6.5. Photoelectric devices

The controllable structure of the AQ backbone offers the potential to enhance light absorption by incorporating different functional group substitutions and applying AQs to photoelectronic devices. Electron-donating substituents (e.g., $-OH$ and $-NH_2$) within the AQ structure can broaden the light absorption range and intensity by modulating the molecular orbital energy [157]. The formation of intramolecular hydrogen bonds in the AQ structure enhances the chromogenic effect [157]. In one study, black polyimides were synthesized through the co-polymerization of 2,4,5,7-tetraamino-1,8-dihydroxyanthracene-9,10-dione with common imine monomers, and these black polyimides were subsequently employed in photoelectronic devices, exhibiting dielectric properties, thermal stability, and strong mechanical properties [157].

3.6.6. Chemical sensors

AQs possess remarkable chromogenic and fluorogenic properties, allowing them to be excited and emit light under visible light with low toxicity. They serve as effective tools for detecting metal ions and are widely used in chemical sensor development [158,159]. For example, Zhao et al. [158] developed an AQ-imidazole-based fluorescent Ag$^+$ sensor for detecting Ag$^+$ ions, demonstrating excellent selectivity and specificity in neutral aqueous solutions. Fluorescent probes based on 2-(1-Amino-2-anthraquinonyliminomethyl) phenol can form complexes with Cu^{2+}, producing highly selective responses [159].

In summary, AQs-based photocatalytic materials have found critical roles in various applications. However, for long-term sustainability, it is crucial to consider the transformation mechanisms and environmental fate of AQs-based composites, especially water-soluble composites, that may pose toxicity risks to organisms after application in environmental settings [160]. Notably, AQs structure containing $-Br$ group exhibit heightened phototoxicity under visible-light irradiation, leading to acute toxic effects observed in organisms such as *Daphnia magna* [161]. The toxicity levels of chemicals are closely linked to their concentrations. Therefore, determining the release of AQs and monitoring their concentrations in both homogeneous and heterogeneous photocatalytic applications (especially environmental pollutant removal) may be essential for minimizing environmental impact while using their beneficial photochemical properties.

4. Immobilization strategy of AQs

AQs exhibit exceptional photochemical and electron transfer properties; however, they suffer from challenges such as low electrical conductivity, limited long-term cycling performance, difficulty separating them during catalytic pollutant degradation, and the potential for secondary contamination [1,43]. To mitigate the environmental impact associated with soluble AQs, researchers have immobilized them on various catalyst supports, including activated carbon felt [162], polyurethane foam [163], ceramsites [164], anion exchange resin [165], metal oxide nanoparticles (e.g.,

Fe_3O_4) [166], MOFs [167], COFs [168], CNTs [169], g-C_3N_4 [38], CDs [101], and graphene [16], using diverse methods. A desirable catalyst carrier should demonstrate high electron mobility, stable physicochemical properties, availability of raw materials, cost-effectiveness, abundant attachment sites, and strong adhesion to the catalyst [170]. Integrating AQs with conductive nanomaterials presents a promising strategy for enhancing conductivity and durability.

The binding mechanism of AQs and supports primarily involves covalent and non-covalent interactions, such as π–π interactions, electrostatic interactions, van der Waals forces, hydrophobic effects, and hydrogen bonding [171]. Covalent functionalization techniques include nucleophilic addition, cycloaddition, radical addition, and electrophilic substitution. Robust interfacial interactions play a crucial role in preventing the agglomerating and leaching of active components, thereby enhancing the stability of the composite [172].

4.1. Covalent interaction

4.1.1. Covalent bonding with graphene-based materials

Among the diverse substrate materials mentioned, graphene consists of 2D nanosheets with a hexagonal structure of sp^2-hybridized carbon atoms, forming delocalized π-electron conjugated units [173]. Graphene exhibits an ultrahigh specific surface area, excellent electrical conductivity, good stability, and facile surface functionalization [174,175]. Chemically modified graphene is synthesized cost-effectively from graphite, graphite oxide, and their derivatives [176]. GO is often preferred as a precursor due to its favorable dispersion in various solvents (e.g., ethanol and water) and its compatibility with organic active components [43]. Treatment of GO with chloroacetic acid and NaOH can increase the number of carboxyl groups. GO reduction with a suitable agent can partially restore graphene's sp^2 structure. Covalent bonding between AQs and graphene primarily involves amide bonding, wherein the amino group of graphene reacts with the carboxyl group of AQ, or vice versa [177]. For example, Lu et al. [178] prepared AQs/reduced graphene oxide (rGO) via a two-step covalent chemical method. Initially, GO was reduced using diethylenetriamine as a reducing agent. The carboxyl and epoxy functional groups of GO can react with the amino functional groups of AQs [179]. Subsequently, the resulting aminated graphene was mixed and reacted with anthraquinone-2-sulfonyl chloride (ASC), yielding AQs combined with graphene composites. Zhang et al. [29] synthesized 2-amino-3-hydroxy-anthraquinone/rGO using a one-step covalent chemical approach under mild water bath conditions (Fig. 8a). Additionally, Qin et al. [31] covalently linked DAAQ molecules to graphene to prevent graphene sheet restacking. DAAQ was converted to an anthraquinone-2,6-diazonium salt, reduced to an aryl radical, and covalently connected to graphene by C—C bonds, forming a porous framework structure [31]. This AQs-loaded graphene material exhibited superior performance compared to graphene in supercapacitors and lithium-ion batteries due to the AQs' redox performance. Zhou et al. [180] modified polyurethane foam (PUF) with AQ2S and rGO, synergistically promoting azo dye biodecolorization. The stable and recyclable AQs—graphene composites connected by covalent bonds exhibit enhanced applicability.

4.1.2. Covalent bonding to other materials

In addition to graphene, AQs can be covalently attached to other carbon material frameworks via diazonium functionalization [181–183]. For instance, using the diazonium coupling method, anthraquinone-1-diazonium chloride•0.5 $ZnCl_2$ (Fast Red AL salt) can be immobilized onto carbon fabric (Spectracarb 2225). Incorporating

AQs into negative electrodes leads to increased average capacitance, energy density, and power duration of the supercapacitors [181]. Furthermore, spontaneous modification of glassy carbon (GC) with AQs was achieved by immersing GC in an acetonitrile solution of AQ diazo derivative (Fast Red AL) [184]. The stability of the modified electrode after 10 min of sonication confirmed the strong binding of Fast Red AL to the electrode. In another approach, 2-aminoanthraquinone can react in $NaNO_2$ and HCl to form diazonium cations, which can then be coupled to the GC electrode via C—C coupling [185]. Similarly, 1-amino-anthraquinone can anchor to the surface of activated carbon through the spontaneous reduction of diazonium cations [182]. The mass ratio of 1-amino-anthraquinone grafted onto carbon material ranged from 0.8% to 14%, influenced by reaction time, amino concentration, and 1-amino-anthraquinone concentration. Notably, the capacitance of the 1-amino-anthraquinone-modified electrode (195 F g^{-1}) exceeded that of the original activated carbon (100 F g^{-1}), attributable to the electrochemically active centers of 1-amino-anthraquinone.

PUF, with its large pore structures, good chemical stability, and low toxicity, serves as a carrier for quinone immobilization, enhancing the decolorization of biological azo dyes [163,186]. AQs can be covalently immobilized on PUF, where ASC reacts with aminated PUF [163]. Similarly, ceramsites, recognized for their light weight, abundant pores, and abundant raw materials, serve as substrates for immobilizing AQs [164]. Ceramsite-supported AQs materials are prepared from amine-functionalized ceramsites (NH_2-ceramsites) using ASC as the raw material [164]. Fe_3O_4, owing to its magnetic properties and ease of preparation and recycling, can also serve as a carrier for AQs through mild covalent chemical methods [166]. The reaction of Fe_3O_4 with carboxylic acid and amino reagents yields carboxylated Fe_3O_4 (Fe_3O_4—COOH) and aminated Fe_3O_4 (Fe_3O_4—NH_2), respectively. Fe_3O_4—COOH reacts with the amino group of the AQ structure, while Fe_3O_4—NH_2 reacts with the carboxyl group, which are connected by amide bonds [166]. In summary, these studies underscore the diverse solid materials that can be covalently bonded to AQs.

4.1.3. Electrochemical methods

When AQs-modified electrodes are applied to electrochemistry, in situ electrochemical approaches are common for preparing composite electrodes. For instance, Maia et al. [187] demonstrated the modification of GC using AQ-COOH in dimethyl sulfoxide and anthraquinone-2-ethanoic acid in N,N-dimethylformamide via electrochemical anodic oxidation. The resulting AQ-COOH-modified electrode exhibited remarkable electrocatalytic ORR activity in an alkaline solution. Conductive polymer-based electrodes, such as polyaniline, polythiophene, and polypyrrole, are also used for electrochemical ORR. Zhang et al. [188] incorporated AQDS into polypyrrole by electropolymerization, adjusting the amount of AQDS through the electropolymerization cycle, resulting in improved performance for the electrogeneration of H_2O_2.

Although covalent functionalization may partially disrupt the conjugated structure of substrate materials, reduce graphene conductivity, and necessitate a tedious preparation process [189,190], incorporating many functional components ensures the stability of the composites.

4.2. Non-covalent interaction

Non-covalent interactions primarily involve forming a new conjugated system through π–π interactions between the AQs and the carbon material. This non-covalent functionalization preserves the conductive properties of the substrates. The strong connection between the AQs and graphene is facilitated by a π-conjugated
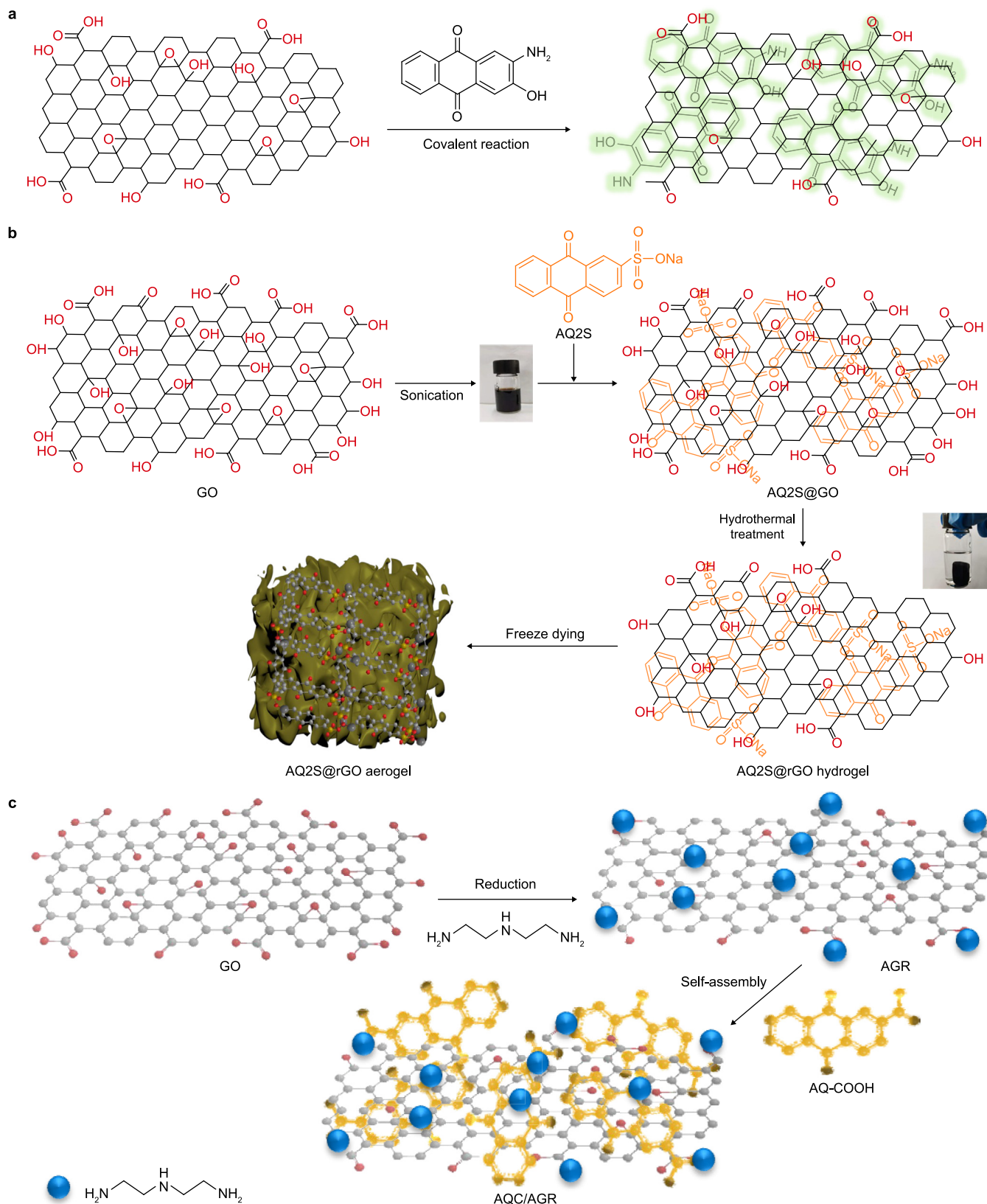
Fig. 8. a, Schematic illustration of the synthesis of 2-amino-3-hydroxy-anthraquinone/rGO. Adapted with permission from Ref. [29]. Copyright 2020, Elsevier B.V. **b**, Schematic illustration of the synthesis of AQ2S@rGO aerogel. Adapted with permission from Ref. [1]. Copyright 2021, Elsevier B.V. **c**, Schematic illustration of AQC/AGR nanosheet synthesis. Adapted with permission from Ref. [16]. Copyright 2023, Elsevier B.V.

system in both materials, enabling robust $\pi{-}\pi$ interactions.

In the adsorption method, AQ or its solution is mixed with a dispersed graphene solution, and the product is obtained via centrifugation or filtration [191,192]. Hydrothermal treatment is a typical laboratory preparation method for achieving non-covalent bonding. Here, GO is the starting precursor, and the defects and oxygen-containing functional groups on GO act as active sites for AQs adsorption during hydrothermal processes [193]. Many of the oxygenated groups on the surfaces of the GO sheets are removed during this reaction. The AQs act as spacers and/or pillars, preventing the aggregation of graphene sheets and resulting in porous and conductive 3D nanostructures [194]. Shi et al. [43] and our group [1] utilized hydrothermal synthesis to immobilize AQ2S on rGO and to prepare 3D interconnected aerogels for supercapacitors and photocatalysts, respectively. Fig. 8b illustrates the preparation process of the aerogel material. The hydrophilicity of the $-SO_3^-$ functional group of AQ2S facilitates binding between AQ2S and rGO at the molecular level [43]. The robust adhesion of AQ2S to rGO via non-covalent $\pi{-}\pi$ stacking effectively inhibits the dissolution of AQ2S in aqueous solution and prevents graphene aggregation. Recently, our group synthesized AQ-COOH-functionalized graphene, specifically aminated graphene coupled with AQ-COOH (Fig. 8c) [16]. Amino functionalization of the GO surface was achieved using a chemical reduction method in which diethylenetriamine acted as the reducing agent and surface modifier. Diethylenetriamine undergoes a nucleophilic ring-opening reaction with the epoxy group of GO to introduce amino groups [195,196]. Consequently, AQ-COOH-functionalized graphene can self-assemble via electrostatic attraction and $\pi{-}\pi$ interactions. Non-covalent functionalization preserves the structure and electronic conductivity of the substrate material, and the preparation process remains relatively straightforward.

4.3. Other methods

4.3.1. Embedding

Enhancing the photostability and reducing the over-aggregation of photosensitizers are key challenges for biological and device applications. Stepwise assembly and modular supramolecular approaches offer promising solutions. Low-toxicity carriers, such as organic dots (ODs), can be created by combining 1,4-diaminoanthraquinone (1,4-AQ), citric acid, and zinc chloride based on coordination, amide, and hydrogen bond interactions [197]. This assembly approach significantly improves the photostability and anti-photooxidation properties of 1,4-AQ. Subsequently, co-assembly with poly(styrene)-*block*-poly(acrylic acid) (PS-*b*-PAA) forms functional dye vesicles. Encapsulation of ODs within nanovesicles at the nanoscale can effectively prevent the deterioration of light-harvesting capability due to 1,4-AQ aggregation (Fig. 9a and b). Incorporating ODs@PS-*b*-PAA vesicles into aqueous polyurethane or polyvinyl alcohol matrices enables the construction of a novel multiband laser-responsive composite [197]. This multistep method enhances the photostability of AQs and offers insights for synthesizing novel photocatalysts.

4.3.2. Anthraquinone-based polymers

Immobilizing AQs on carbon materials for lithium-ion battery applications often results in unsatisfactory long-term cycling performance [198]. Therefore, an alternative approach is to utilize insoluble compounds comprising quinone moieties that meet energy density and cycle life requirements. AQ-based polymers exhibit superior electrochemical properties, high stabilities, structural diversity, and improved redox kinetics [198–200]. π-Conjugated polyanthraquinones are synthesized through the organometallic dehalogenation polycondensation method [201].
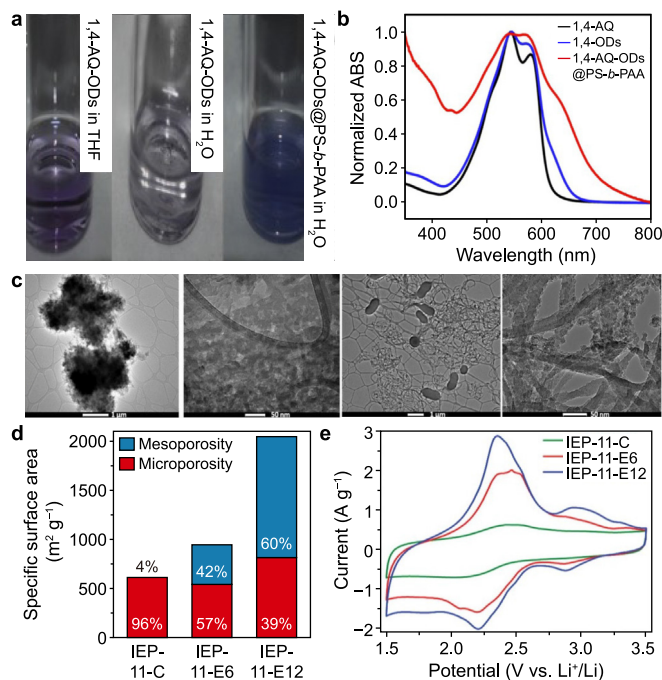
Fig. 9. a, Photograph of 1,4-AQ-ODs in tetrahydrofuran (THF) and aqueous solution, and 1,4-AQ-ODs@PS-b-PAA in aqueous solution. **b**, UV−vis absorption spectra of 1,4-AQ in THF solution, 1,4-AQ-ODs in THF solution, and 1,4-AQ-ODs@PS-b-PAA vesicles in aqueous solution. Adapted with permission from Ref. [197]. Copyright 2021, American Chemical Society. **c**, Transmission electron microscope images at different magnifications of IEP-11-C (the first two) and IEP-11-E12 (the last two). **d**, Percentages of microporosity and mesoporosity for IEP-11-C, IEP-11-E6, and IEP-11-E12. **e**, Cycling voltammetry of AQ-based CMPs. Adapted with permission from Ref. [199]. Copyright 2019, Wiley.

For example, 1-chloroanthraquinone as a feedstock yields polyanthraquinones via C−C coupling catalyzed by a zero-valent NiL_m complex, where NiL_m consists of bis(1,5-cyclooctadiene)nickel(0) Ni(cod)$_2$ and 2,2′-bipyridine (bpy) [201]. In addition to forming polymers by their polymerization reactions, AQs can also form D–A conjugated polymers. AQs' redox properties and electron deficiency make them valuable in D–A conjugated polymers, where they can serve as both electron acceptors and mediators of electron transfer [26,136,202,203]. A conjugated microporous polymer (CMP) can be synthesized via a Pd-catalyzed Suzuki-Miyaura reaction between D and A precursors, forming C−C bonds coupling in a one-pot reaction [202]. Additionally, D−A CMP is prepared by polycondensation of 2,5,8,11-tetrakis (4,4,5,5-tetramethyl-1,3,2-dioxaborolan-2-yl) perylene with 2,6-dibromoanthraquinone, where the perylene moiety functions as an electron donor, and AQ functions as an electron acceptor [26]. Structural characterization has been employed to confirm successful CMP synthesis [26]. In the CMP system, the built-in electric field and AQ-induced intermolecular charge transfer play critical roles in the photocatalytic reduction of uranium(VI) (UO_2^{2+}) to UO_2 in strongly acidic solutions (pH 1) [26]. Furthermore, Molina et al. [199] reported a two-step pathway combining miniemulsion polymerization and subsequent solvothermal treatment via a Sonogashira cross-coupling reaction to synthesize an AQ-based CMP. Compared to the traditional Sonogashira approach (IEP-11-C), the AQ-based CMPs (IEP-11-E6 and IEP-11-E12) obtained through this method exhibited altered morphology, structure, and excellent electrochemical activity (Fig. 9c−e). DAAQ can also be a raw material for synthesizing COF linked to 1,3,5-triformylresorcinol via C═N bonds through Schiff base condensation reactions [146,204]. The resulting AQ-COF is

chemically and thermally stable, insoluble in common solvents, and exhibits a specific surface area of 609 m^2 g^{-1} [146].

4.4. Recyclability of photocatalysts

The stability and reusability of photocatalysts are critical factors in assessing their performance for practical applications. Researchers typically evaluate material stability through multiple cycling experiments, scanning electron microscopy, X-ray diffraction patterns, fourier transform infrared spectra, and other characterization methods. Changes in morphology, crystalline structure, functional groups, and other photocatalyst characteristics are observed before and after use.

Magnetic photocatalysts are typically recovered magnetically, employing materials such as ZnFe$_2$O$_4$, known for their responsiveness to visible light, chemical stability, and magnetic recyclability [205]. Le et al. [205] synthesized a Z-type photocatalyst (ZnFe$_2$O$_4$/g-C$_3$N$_4$) via a hydrothermal method for the removal of Cr(VI) and As(III). The reduction of Cr(VI) and As(III) remained efficient even after multiple cycles, and X-ray diffraction patterns and scanning electron microscopy confirmed that the photocatalyst was extremely stable. In addition to ZnFe$_2$O$_4$, magnetic CoFe$_2$O$_4$ [206], Fe$_3$O$_4$ [207], and MgFe$_2$O$_4$ [208] are commonly utilized in various photocatalytic applications. For instance, Feng et al. [206] developed a dual-Z-type heterojunction photocatalyst (GCNQDs-CoTiO$_3$/CoFe$_2$O$_4$) with desirable magnetic properties and conducted a four-cycle stability experiment. The oxytetracycline removal rate remained above 85% after four cycles, indicating good stability. X-ray diffraction patterns showed no significant changes before and after oxytetracycline degradation, and no stray peaks, and scanning electron microscopy and transmission electron microscope image characterizations revealed minimal alterations, confirming material stability. Magnetic properties were evaluated using a vibrating sample magnetometer, showing increased saturation magnetization intensity with higher Co content for effective separation using a magnet. Thus, these magnetic properties facilitate convenient catalyst recycling.

For non-magnetic photocatalysts, recovery methods mainly include centrifugation and filtration. For instance, Yu et al. [26] demonstrated the stability and reusability of D–A CMP-containing AQ through five cycles of U(VI) photoreduction. Wang et al. [209] designed an AQ-based Cu(I) cyclic trinuclear complex that exhibited excellent reusability over ten cycles for C–C coupling reactions. Notably, to optimize the separation and recovery of non-magnetic photocatalysts, they can be loaded onto blocks [210,211] or membrane materials [212,213] to enable continuous operation. Unlike 2D graphene nanosheets, 3D crosslinked graphene gels offer a porous structure with macrostructural stability, providing more active sites for photocatalytic reactions while facilitating easy separation from the reaction solution to minimize contamination [214]. In addition, 3D block sponge carriers, such as melamine and polyurethane, are known for their high porosity, low density, and cost-effectiveness for photocatalytic pollutant removal and other applications [210]. For example, Li et al. [215] reported a strategy for preparing photocatalyst coatings on polyurethane sponges using a powder-spraying method for intimately coupled photocatalysis and biodegradation, and these photocatalytic carriers exhibited excellent stability. These preparation strategies, which involve imparting magnetic properties and anchoring powdered catalysts onto carriers, are superior for practical applications and recycling processes.

5. Conclusions and perspectives

AQs exhibit remarkable redox-active and photosensitive properties, making AQs-based photocatalysts extensively utilized in diverse fields, such as medicine, energy, optics, and environmental pollutant remediation. A significant advantage of AQs is their controllable structural modifications, influencing their redox and photochemical behaviors. By introducing different substituents (electron-withdrawing or electron-donating groups), AQs can exhibit varied optical absorption and redox potentials. This review has elucidated the multifaceted roles of AQs in photocatalytic systems, including mediating charge transfer, acting as light-absorbing components, and enhancing the generation of reactive species. When integrated into semiconductor materials, AQs primarily function as charge-transport mediators and electron acceptors while serving as the primary photoactive components in other scenarios, facilitating the generation of reactive species upon illumination. Moreover, this review has discussed the applications of AQs-based photocatalytic systems in H$_2$O$_2$ production, pollutant degradation, H$_2$ evolution, and bacterial inactivation. The efficiencies and mechanisms of these photocatalytic applications have been adequately examined. Particularly notable is the interaction of photoexcited AQs with Cl$^-$ in water via charge-transfer interactions, promoting the generation of ROS and RCS, thereby facilitating the degradation of organic pollutants. Finally, strategies and methods for integrating AQs with solid carriers to construct AQs-based composites are presented. The findings highlight that coupling AQs with graphene can significantly enhance the transfer of photogenerated carriers, thereby boosting the photocatalytic activity and durability of composite photocatalysts. However, for future research in AQs-based photocatalytic technology, several critical aspects and development directions require in-depth investigation.

(1) A systematic investigation of the structure and characteristics of AQs is crucial for optimizing photocatalytic activity. The impact of grafting different functional groups on the light absorption and electron transfer abilities of AQs requires further exploration.

(2) Addressing the poor conductivity and homogeneity of AQs is essential for practical applications, particularly in wastewater treatment. Grafting AQs onto solid matrices is essential to maintaining their activity and enhancing recyclability. It is necessary to assess the stability of photocatalysts by employing various morphological and structural characterization tools.

(3) Although AQs demonstrate promising potential for photocatalytic pollutant degradation in water containing Cl$^-$, the potential generation of free chlorine during reactions may lead to halogenated byproducts. Therefore, future research should focus on designing photocatalysts for highly selective pollutant degradation to minimize halogenated product formation.

(4) The long-term stability and repeatability of AQs-based photocatalysts may be considered in future studies, as well as evaluating their applicability in real wastewater treatment scenarios.

In addressing these research challenges, several potential solutions and approaches are proposed.

(1) Machine learning methods can model and analyze complex multidimensional data, such as the elemental composition and structural characterization of AQs-based catalysts. This method can expedite the structure–performance relationship analysis, leading to the development of novel functional material with tailored properties. TD-DFT calculations can also be employed to analyze the excited state and electronic properties of AQs with different structures, aiding in

predicting photoactivity and understanding catalytic mechanisms. Combining DFT with experiments can simplify the research system efficiently and reliably.

(2) There are diverse substrates and strategies available for preparing AQs-based composites. Influencing factors, such as size, reaction site, crystalline surface, specific surface area, and bonding type, need to be carefully considered when designing substrate structures suitable for various photocatalytic applications. Future studies should evaluate how different composite dimensions affect the physical and chemical properties of catalysts and their photocatalytic activity. Considering the photocatalyst recovery, preparing macroscopic catalysts for easy recycling and continuous operation may be a good approach. Graphene materials with high specific surface areas, tunable structures, and excellent electron-transfer properties are expected to open up new possibilities for the development of innovative AQs-based photocatalytic architectures through the design of interfacial bonds between AQs and graphene and the modulation of carrier migration efficiency.

(3) By adjusting the structure of AQs-based materials, it may be possible to emphasize non-radical mechanisms to mitigate the detrimental effects of Cl^- during pollutant transformations in aqueous environments. Further, photocatalysis should be coupled with other processes, such as electrochemical and Fenton-like processes, to produce photoelectrocatalytic reactions by adding electrodes or light-assisted Fenton-like reactions by introducing peroxides (H_2O_2 and persulfate). It is desirable that these coupling techniques promote the production of powerful reactive species, improve pollutant removal, and maximize the synergistic effect between them. These approaches require consideration of the complex catalytic mechanism and the nature of the pollutants being treated.

(4) To advance the practical application of AQs-based photocatalysts, loading AQs into macroscopic carriers and developing catalytic membranes are essential to improve the long-term sustainability of immobilized AQs photocatalysts. Moreover, we anticipate future research considering the configuration of the photocatalytic reactor with the state of the photocatalysts (suspended or immobilized), the effective use of light by the photocatalysts, the sufficiency of the contact between the photocatalysts and pollutants, and the enhancement of the mass transfer efficiency. In addition, there is a need to explore the effects of real wastewater parameters on the pollutant degradation performance of AQs-based photocatalytic technologies, which is important for the design and development of catalysts suitable for practical applications.

CRediT authorship contribution statement

Cheng-Xin Chen: Writing - Review & Editing, Writing - Original Draft, Methodology, Investigation, Data Curation, Conceptualization. **Shan-Shan Yang:** Writing - Review & Editing, Validation, Conceptualization. **Ji-Wei Pang:** Validation, Investigation. **Lei He:** Writing - Review & Editing, Methodology, Investigation. **Ya-Ni Zang:** Validation, Investigation. **Lan Ding:** Software, Methodology. **Nan-Qi Ren:** Writing - Review & Editing, Supervision. **Jie Ding:** Writing - Review & Editing, Validation, Supervision.

Declaration of competing interest

The authors declare that they have no known competing financial interests or personal relationships that could have appeared to influence the work reported in this paper.

References

[1] C. Chen, S. Yang, J. Ding, G. Wang, L. Zhong, S. Zhao, Y. Zang, J. Jiang, L. Ding, Y. Zhao, L. Liu, N. Ren, Non-covalent self-assembly synthesis of AQ2S@rGO nanocomposite for the degradation of sulfadiazine under solar irradiation: the indispensable effect of chloride, Appl. Catal. B Environ. 298 (2021) 120495.

[2] H.B. Truong, T.T.L. Doan, N.T. Hoang, N. Van Tam, M.K. Nguyen, L.G. Trung, J.S. Gwag, N.T. Tran, Tungsten-based nanocatalysts with different structures for visible light responsive photocatalytic degradation of bisphenol A, J. Environ. Sci. 139 (2024) 569−588.

[3] H. Fu, Y. Deng, Z. Cai, Y. Pan, L. Yang, T. Fujita, N. Wang, Y. Wang, X. Wang, Designing Z-scheme In_2O_3 @$ZnIn_2S_4$ core-shell heterojunctions for enhanced photocatalytic multi-pollutant removal, J. Hazard Mater. 463 (2024) 132820.

[4] C. Maggu, S. Singla, S. Basu, Unleashing the power of sunlight: Bi_2O_3/Sb_2S_3 photocatalysis for sustainable wastewater remediation of Tetracycline and Rhodamine-B, J. Environ. Manag. 349 (2024) 119424.

[5] L.J. Chen, Y.L. Chuang, T.B. Nguyen, C.W. Chen, C.D. Dong, Enhanced photocatalytic activity of tin oxide-doped molybdenum disulfide nanohybrids under visible light irradiation: antibiotics elimination, heavy metal reduction and antibacterial behavior, Environ. Res. 238 (2023) 117259.

[6] D. Li, Y. Wang, X. Qi, W. Huang, Y. Wang, X. Zhao, Y. Liu, X. Song, X. Cao, A photocatalytic-microbial coupling system for simultaneous removal of harmful algae and enhanced denitrification: construction, performance and mechanism of action, J. Hazard Mater. 459 (2023) 132233.

[7] S.H. Paiman, S.F. Md Noor, N. Ngadi, A.H. Nordin, N. Abdullah, Insight into photocatalysis technology as a promising approach to tackle microplastics pollution through degradation and upcycling, Chem. Eng. J. 467 (2023) 143534.

[8] A. Fujishima, K. Honda, Electrochemical photolysis of water at a semiconductor electrode, Nature 238 (5358) (1972) 37−38.

[9] M.N. Chong, B. Jin, C.W.K. Chow, C. Saint, Recent developments in photocatalytic water treatment technology: a review, Water Res. 44 (10) (2010) 2997−3027.

[10] N. Naeinian, M. Imani, A. Tadjarodi, Mechanochemical synthesis of $CoFe_2O_4/Bi_2MoO_6$ mixed metal oxide and study of its photocatalytic behavior, Mater. Lett. 355 (2024) 135512.

[11] A. Chawla, A. Sudhaik, Sonu, P. Raizada, T. Ahamad, Q.V. Le, V.-H. Nguyen, S. Thakur, A.K. Mishra, R. Selvasembian, P. Singh, Bi-rich $Bi_xO_yBr_z$-based photocatalysts for energy conversion and environmental remediation: a review, Coord. Chem. Rev. 491 (2023) 215246.

[12] Y. Zhi, S. Ma, H. Xia, Y. Zhang, Z. Shi, Y. Mu, X. Liu, Construction of donor-acceptor type conjugated microporous polymers: a fascinating strategy for the development of efficient heterogeneous photocatalysts in organic synthesis, Appl. Catal. B Environ. 244 (2019) 36−44.

[13] Y.X. Chen, Y.M. Yuan, H.Y. Yang, Q. Wang, Y. Ren, X.H. Guo, P. Zhang, M.J. Zhang, W. Wang, L.Y. Chu, Hierarchical porous tannic-acid-modified MOFs/alginate particles with synergized adsorption-photocatalysis for water remediation, Sep. Purif. Technol. 330 (2024) 125435.

[14] L. Jian, Y. Dong, H. Zhao, C. Pan, G. Wang, Y. Zhu, Highly crystalline carbon nitrogen polymer with a strong built-in electric fields for ultra-high photocatalytic H_2O_2 production, Appl. Catal. B Environ. 342 (2024) 123340.

[15] H. Hu, Y. Hu, W. Kong, Y. Tao, Q. Jiang, J. Wang, C. Li, H. Xie, Y. Shi, Y. Li, G. Chen, J. Liang, S. Zhou, Y. Kong, Y. Zhu, The photocatalytic mineralization of phenolic wastewater via self-generation and -activation of H_2O_2 technology, J. Environ. Chem. Eng. 11 (5) (2023) 111108.

[16] C.X. Chen, S.S. Yang, J. Ding, L. Ding, R. Wu, L.M. Liu, J.W. Pang, L. He, J.Q. Jiang, N.Q. Ren, Existence of chloride ions in high salinity wastewater accelerates the removal of micropollutants over light-driven catalysts, Appl. Catal. B Environ. 334 (2023) 122823.

[17] Y. Gong, Y. Ding, Q. Tang, F. Lian, C. Bai, R. Xie, H. Xie, X. Zhao, Plasmonic Ag nanoparticles decorated MIL-101(Fe) for enhanced photocatalytic degradation of bisphenol A with peroxymonosulfate under visible-light irradiation,

Chin. Chem. Lett. 35 (1) (2024) 108475.

[18] A. Mahmoud Idris, S. Zheng, L. Wu, S. Zhou, H. Lin, Z. Chen, L. Xu, J. Wang, Z. Li, A heterostructure of halide and oxide double perovskites Cs$_2$AgBiBr$_6$/ Sr$_2$FeNbO$_6$ for boosting the charge separation toward high efficient photocatalytic CO$_2$ reduction under visible-light irradiation, Chem. Eng. J. 446 (2022) 137197.

[19] Y. Guo, B. Liu, J. Zhang, G. Wang, C. Pan, H. Zhao, C. Wang, F. Yu, Y. Dong, Y. Zhu, Perylene imide supermolecule promote oxygen to superoxide radical for ultrafast photo-oxidation of 5-hydroxymethylfurfural, Appl. Catal. B Environ. 340 (2024) 123217.

[20] Z. Wang, Z. Liu, J. Huang, Y. Chen, R. Su, J. He, G. Lv, B. Gao, W. Zhou, Y. Wang, Z. Wang, Q. Li, Zr$_6$O$_8$-porphyrinic MOFs as promising catalysts for the boosting photocatalytic degradation of contaminants in high salinity wastewater, Chem. Eng. J. 440 (2022) 135883.

[21] E. Vargas, R. Vargas, O. Nunez, A TiO$_2$ surface modified with copper(II) phthalocyanine-tetrasulfonic acid tetrasodium salt as a catalyst during photoinduced dichlorvos mineralization by visible solar light, Appl. Catal. B Environ. 156 (2014) 8−14.

[22] B. Yan, J. Peng, F. Deng, L. Liu, X. Li, P. Shao, J. Zou, S. Zhang, J. Wang, X. Luo, Novel ZnFe$_2$O$_4$/Bi$_2$S$_3$ high-low junctions for boosting tetracycline degradation and Cr(VI) reduction, Chem. Eng. J. 452 (2023) 139353.

[23] R. Greco, L. Baxauli-Marin, F. Temerov, M. Daboczi, S. Eslava, Y. Niu, A. Zakharov, M. Zhang, T. Li, W. Cao, Activation of 2D cobalt hydroxide with 0D cobalt oxide decoration for microplastics degradation and hydrogen evolution, Chem. Eng. J. 471 (2023) 144569.

[24] L. Yue, M. Tao, L. Xu, C. Wang, Y. Xu, Y. Liu, X. Cao, J.C. White, Z. Wang, Size-dependent photocatalytic inactivation of *Microcystis aeruginosa* and degradation of microcystin by a copper metal organic framework, J. Hazard Mater. 462 (2024) 132799.

[25] D. Jiang, Q. Zhang, L. Yang, Y. Deng, B. Yang, Y. Liu, C. Zhang, Z. Fu, Regulating effects of anthraquinone substituents and additives in photo-catalytic oxygenation of *p*-xylene by molecular oxygen under visible light irradiation, Renew. Energy 174 (2021) 928−938.

[26] F. Yu, Z. Zhu, C. Li, W. Li, R. Liang, S. Yu, Z. Xu, F. Song, Q. Ren, Z. Zhang, A redox-active perylene-anthraquinone donor-acceptor conjugated microporous polymer with an unusual electron delocalization channel for photocatalytic reduction of uranium (VI) in strongly acidic solution, Appl. Catal. B Environ. 314 (2022) 121467.

[27] V. Hasija, P. Singh, S. Thakur, K. Stando, V.H. Nguyen, Q.V. Le, S.M. Alshehri, T. Ahamad, K.C.W. Wu, P. Raizada, Oxygen doping facilitated N-vacancies in g-C$_3$N$_4$ regulates electronic band gap structure for trimethoprim and Cr (VI) mitigation: Simulation studies and photocatalytic degradation pathways, Appl. Mater. Today 29 (2022) 101676.

[28] J. Cervantes González, D.A. Vosburg, S.E. Mora Rodriguez, M.A. Vázquez, L.G. Zepeda, C. Villegas Gómez, S. Lagunas Rivera, Anthraquinones: versatile organic photocatalysts, ChemCatChem 12 (15) (2020) 3811−3827.

[29] H. Zhang, K. Han, X. Hu, Enhanced bioreduction of 2,5-dichlorobenzene by an AHQ/RGO binary nanocomposite through a synergistic effect with outer membrane proteins of *Shewanella oneidensis* MR-1, Chem. Eng. J. 389 (2020) 124464.

[30] J. Xu, J. Xie, Y. Wang, L. Xu, Y. Zong, W. Pang, L. Xie, Effect of anthraquinone-2,6-disulfonate (AQDS) on anaerobic digestion under ammonia stress: Triggering mediated interspecies electron transfer (MIET), Sci. Total Environ. 828 (2022) 154158.

[31] Y. Qin, J.M. Li, X. Jin, S.H. Jiao, Y.W. Chen, W.B. Cai, R.G. Cao, Anthraquinone-functionalized graphene framework for supercapacitors and lithium batteries, Ceram. Int. 46 (10) (2020) 15379−15384.

[32] S. Abbasi, F. Hekmat, S. Shahrokhian, Dual redox electrolytes for improving the performance of asymmetric supercapacitors constructed from heteroatom-doped green carbon spheres, J. Alloys Compd. 957 (2023) 170452.

[33] I. Loeff, A. Treinin, H. Linschitz, The photochemistry of 9,10-anthraquinone-2-sulfonate in solution. 2. Effects of inorganic anions: quenching vs. radical formation at moderate and high anion concentrations, J. Phys. Chem. 88 (21) (1984) 4931−4937.

[34] I. Loeff, S. Goldstein, A. Treinin, H. Linschitz, Interactions of formate ion with triplets on anthraquinone-2-sulfonate, 1,4-naphthoquinone, benzophenone-4-carboxylate, and benzophenone-4-sulfonate, J. Phys. Chem. 95 (11) (1991) 4423−4430.

[35] N.A. Romero, D.A. Nicewicz, Organic photoredox catalysis, Chem. Rev. 116 (17) (2016) 10075−10166.

[36] I. Loeff, J. Rabani, A. Treinin, H. Linschitz, Charge-transfer and reactivity of nπ* and ππ* organic triplets, including anthraquinonessulfonates, in interactions with inorganic anions: a comparative-study based on classical marcus theory, J. Am. Chem. Soc. 115 (20) (1993) 8933−8942.

[37] I. Ghosh, Excited radical anions and excited anions in visible light photoredox catalysis, Phys. Sci. Rev. 4 (12) (2019) 20170185.

[38] Y. Ye, C. Wen, J. Pan, J. Wang, Y. Tong, S. Wei, Z. Ke, L. Jiang, F. Zhu, N. Zhou, M. Zhou, J. Xu, G. Ouyang, Visible-light driven efficient overall H$_2$O$_2$ production on modified graphitic carbon nitride under ambient conditions, Appl. Catal. B Environ. 285 (2021) 119726.

[39] R.C. de Souza Oliveira, R.J. Corrêa, R.S.P. Teixeira, D.D. Queiroz, R. da Silva Souza, S.J. Garden, N.C. de Lucas, M.D. Pereira, J.S. Bello Forero, E.C. Romani, E.S. Ribeiro, Silica nanoparticles doped with anthraquinone for lung cancer phototherapy, J. Photochem. Photobiol., B 165 (2016) 1−9.

[40] L. Zhang, P. Chen, Y. Xu, W. Nie, Y. Zhou, Enhanced photo-induced antibacterial application of graphene oxide modified by sodium anthraquinone-2-sulfonate under visible light, Appl. Catal. B Environ. 265 (2020) 118572.

[41] L. He, S.-S. Yang, J. Ding, Z.-L. He, J.-W. Pang, D.-F. Xing, L. Zhao, H.-S. Zheng, N.-Q. Ren, W.-M. Wu, Responses of gut microbiomes to commercial polyester polymer biodegradation in Tenebrio molitor Larvae, J. Hazard Mater. 457 (2023) 131759.

[42] J. Gacs, W.Y. Zhang, T. Knaus, F.G. Mutti, I. Arends, F. Hollmann, A photoenzymatic cascade to transform racemic alcohols into enantiomerically pure amines, Catalysts 9 (4) (2019) 11.

[43] R.Y. Shi, C.P. Han, H. Duan, L. Xu, D. Zhou, H.F. Li, J.Q. Li, F.Y. Kang, B.H. Li, G.X. Wang, Redox-active organic sodium anthraquinone-2-sulfonate (AQS) anchored on reduced graphene oxide for high-performance supercapacitors, Adv. Energy Mater. 8 (31) (2018) 1802088.

[44] M. Yusuf, I. Solanki, P. Jain, R. Kumar, Photochemical studies: Chromones, bischromones and anthraquinone derivatives, Arab. J. Chem. 12 (7) (2019) 1197−1211.

[45] M. Nowak-Perlak, P. Ziółkowski, M. Woźniak, A promising natural anthraquinones mediated by photodynamic therapy for anti-cancer therapy, Phytomedicine 119 (2023) 155035.

[46] S. Zhu, S. Zhu, F. Xing, Anthraquinone-1,8-derived (pseudo-) crown and lariat ethers:Design and applications as fluorescent and chromogenic ion (pair) sensors, Chem. Asian J. 17 (17) (2022) e202200564.

[47] F. Dumur, Recent advances on anthraquinone-based photoinitiators of polymerization, Eur. Polym. J. 191 (2023) 112039.

[48] E. Gómez Alvarez, H. Wortham, R. Strekowski, C. Zetzsch, S. Gligorovski, Atmospheric photosensitized heterogeneous and multiphase reactions: from outdoors to indoors, Environ. Sci. Technol. 46 (4) (2012) 1955−1963.

[49] X. Duan, Z. Zhou, X. Huang, Z. Qu, Generation of singlet oxygen catalyzed by the room-temperature-stable anthraquinone anion radical, Phys. Chem. Chem. Phys. 24 (23) (2022) 14165−14171.

[50] J.M. Anglada, M.T.C. Martins Costa, J.S. Francisco, M.F. Ruiz López, Photoinduced oxidation reactions at the air−water interface, J. Am. Chem. Soc. 142 (38) (2020) 16140−16155.

[51] S.C. Núñez Montoya, L.R. Comini, M. Sarmiento, C. Becerra, I. Albesa, G.A. Argüello, J.L. Cabrera, Natural anthraquinones probed as Type I and Type II photosensitizers: singlet oxygen and superoxide anion production, J. Photochem. Photobiol., B 78 (1) (2005) 77−83.

[52] F. Wilkinson, W.P. Helman, A.B. Ross, Quantum yields for the photosensitized formation of the lowest electronically excited singlet state of molecular oxygen in solution, J. Phys. Chem. Ref. Data 22 (1) (1993) 113−262.

[53] M.J. Frisch, G.W. Trucks, H.B. Schlegel, G.E. Scuseria, M.A. Robb, J.R. Cheeseman, G. Scalmani, V. Barone, G.A. Petersson, H. Nakatsuji, X. Li, M. Caricato, A.V. Marenich, J. Bloino, B.G. Janesko, R. Gomperts, B. Mennucci, H.P. Hratchian, J.V. Ortiz, A.F. Izmaylov, J.L. Sonnenberg, D. Williams Young, F. Ding, F. Lipparini, F. Egidi, J. Goings, B. Peng, A. Petrone, T. Henderson, D. Ranasinghe, V.G. Zakrzewski, J. Gao, N. Rega, G. Zheng, W. Liang, M. Hada, M. Ehara, K. Toyota, R. Fukuda, J. Hasegawa, M. Ishida, T. Nakajima, Y. Honda, O. Kitao, H. Nakai, T. Vreven, K. Throssell, J.A. Montgomery, J.E. Peralta, F. Ogliaro, M.J. Bearpark, J.J. Heyd, E.N. Brothers, K.N. Kudin, V.N. Staroverov, T.A. Keith, R. Kobayashi, J. Normand, K. Raghavachari, A.P. Rendell, J.C. Burant, S.S. Iyengar, J. Tomasi, M. Cossi, J.M. Millam, M. Klene, C. Adamo, R. Cammi, J.W. Ochterski, R.L. Martin, K. Morokuma, O. Farkas, J.B. Foresman, D.J. Fox, Gaussian 16, Gaussian, Inc., Wallingford CT, 2016.

[54] R.S. Mulliken, Electronic population analysis on LCAO−MO molecular wave functions. I, J. Chem. Phys. 23 (10) (1955) 1833−1840.

[55] A.D. Becke, A new mixing of Hartree−Fock and local density-functional theories, J. Chem. Phys. 98 (2) (1993) 1372−1377.

[56] A.D. Becke, Density-functional thermochemistry. III. The role of exact exchange, J. Chem. Phys. 98 (7) (1993) 5648−5652.

[57] S. Grimme, S. Ehrlich, L. Goerigk, Effect of the damping function in dispersion corrected density functional theory, J. Comput. Chem. 32 (7) (2011) 1456−1465.

[58] S. Miertuš, E. Scrocco, J. Tomasi, Electrostatic interaction of a solute with a continuum. A direct utilizaion of AB initio molecular potentials for the prevision of solvent effects, Chem. Phys. 55 (1) (1981) 117−129.

[59] E. Cancès, B. Mennucci, J. Tomasi, A new integral equation formalism for the polarizable continuum model: theoretical background and applications to isotropic and anisotropic dielectrics, J. Chem. Phys. 107 (8) (1997) 3032−3041.

[60] M. Feng, R. Zeng, S.L. Chou, F.L. Gu, Enhancing the understanding of the redox properties of lithium-inserted anthraquinone derivatives by regulating molecular structure, J. Electroanal. Chem. 887 (2021) 115172.

[61] V.J.P. Srivatsavoy, B. Venkataraman, N. Periasamy, The deexcitation of the S$_1$ state of aminoanthraquinones: a steadystate and timeresolved study, Proc. Indian Acad. Sci. 104 (6) (1992) 731−737.

[62] J. Guo, J. Lian, Y. Guo, X. Liu, C. Zhang, L. Yue, Y. Wang, Redox activity and accelerating capacity of model redox mediators during biodenitrification, Biotechnol. Biotechnol. Equip. 29 (4) (2015) 673−679.

[63] X. Yang, Y. Wang, C. Zhang, T. Fang, L. Zhou, W. Zhang, J. Xu, Steric effects of substituents of quinones on the oxygenation of ethylbenzene catalyzed by NHPI/quinone and the catalytic oxidation of ascorbate, J. Phys. Org. Chem. 24 (8) (2011) 693−697.

[64] F. Amano, Y. Akaki, A. Yamakata, Effects of hydroxy groups in anthraquinone dyes on photocatalytic activity of visible-light-sensitized Pt-TiO$_2$ for

hydrogen evolution, Catal. Surv. Asia 27 (1) (2023) 75–83.

[65] L. Zhou, Y. Chen, X. Yang, Y. Su, W. Zhang, J. Xu, Electronic effect of sub-stituent of quinones on their catalytic performance in hydrocarbons oxida-tion, Catal. Lett. 125 (1) (2008) 154–159.

[66] S. Liao, J. Liu, L. Yan, Q. Liu, G. Chen, L. Ma, 2-Bromoanthraquinone as a highly efficient photocatalyst for the oxidation of sec-aromatic alcohols: experi-mental and DFT study, RSC Adv. 10 (61) (2020) 37014–37022.

[67] H. Yin, Y. Yuan, Y. Li, J. Tang, W. Zhong, L. Mao, Enhanced driving force and charge separation efficiency of protonated anthraquinone for C–H photo-oxygenation of alkanes by proton-coupled electron transfer, Green Chem. 25 (7) (2023) 2757–2770.

[68] N. Liu, G. Sun, Production of reactive oxygen species by photoactive anthraquinone compounds and their applications in wastewater treatment, Ind. Eng. Chem. Res. 50 (9) (2011) 5326–5333.

[69] M. Le Bechec, T. Pigot, S. Lacombe, Chemical quenching of singlet oxygen and other reactive oxygen species in water: a reliable method for the determi-nation of quantum yields in photochemical processes? Chemphotochem 2 (7) (2018) 622–631.

[70] S. Garg, A.L. Rose, T.D. Waite, Production of reactive oxygen species on photolysis of dilute aqueous quinone solutions, Photochem. Photobiol. 83 (4) (2007) 904–913.

[71] F. Ronzani, N. Costarramone, S. Blanc, A.K. Benabbou, M.L. Bechec, T. Pigot, M. Oelgemöller, S. Lacombe, Visible-light photosensitized oxidation of α-terpinene using novel silica-supported sensitizers: photooxygenation vs. photodehydrogenation, J. Catal. 303 (2013) 164–174.

[72] C. Cantau, T. Pigot, N. Manoj, E. Oliveros, S. Lacombe, Singlet oxygen in microporous silica xerogel: quantum yield and oxidation at the gas–solid interface, ChemPhysChem 8 (16) (2007) 2344–2353.

[73] J. Zhuo, Photochemical Study of Anthraquinone Derivatives and Their Ap-plications, University of California, United States, 2016.

[74] S.H. Cho, H. Huh, H.M. Kim, C.I. Kim, N.J. Kim, S.K. Kim, Laser induced fluo-rescence and resonant two-photon ionization spectroscopy of jet-cooled 1-hydroxy-9,10-anthraquinone, J. Chem. Phys. 122 (3) (2005) 034304.

[75] L. Cui, S. Furuhashi, Y. Tachikawa, N. Tada, T. Miura, A. Itoh, Efficient gen-eration of hydrogen peroxide by aerobic photooxidation of 2-propanol using anthraquinone-2-carboxylic acid and one-pot epoxidation of α,β-unsatu-rated ketones, Tetrahedron Lett. 54 (2) (2013) 162–165.

[76] N. Liu, G. Sun, Photoinduced decolorization of 2, 6-dichloroindophenol by 2-anthraquinone sulfonate treated nylon, ACS Appl. Mater. Interfaces 3 (4) (2011) 1221–1227.

[77] N. Liu, G. Sun, J. Zhu, Photo-induced self-cleaning functions on 2-anthraquinone carboxylic acid treated cotton fabrics, J. Mater. Chem. 21 (39) (2011) 15383–15390.

[78] A. Gao, H. Zhang, G. Sun, K. Xie, A. Hou, Light-induced antibacterial and UV-protective properties of polyamide 56 biomaterial modified with anthra-quinone and benzophenone derivatives, Mater. Des. 130 (2017) 215–222.

[79] D. Vione, P.R. Maddigapu, E. De Laurentiis, M. Minella, M. Pazzi, V. Maurino, C. Minero, S. Kouras, C. Richard, Modelling the photochemical fate of ibuprofen in surface waters, Water Res. 45 (20) (2011) 6725–6736.

[80] G. Marchetti, M. Minella, V. Maurino, C. Minero, D. Vione, Photochemical transformation of atrazine and formation of photointermediates under conditions relevant to sunlit surface waters: laboratory measures and modelling, Water Res. 47 (16) (2013) 6211–6222.

[81] P.R. Maddigapu, C. Minero, V. Maurino, D. Vione, M. Brigante, G. Mailhot, Enhancement by anthraquinone-2-sulphonate of the photonitration of phenol by nitrite: Implication for the photoproduction of nitrogen dioxide by coloured dissolved organic matter in surface waters, Chemosphere 81 (11) (2010) 1401–1406.

[82] A.M. Lastre-Acosta, C.M. Rocha, M.A. Mendes, A.C.S.C. Teixeira, C.A.O. do Nascimento, Sunlight-driven environmental photodegradation of 2-chlorobiphenyl (PCB-1) in surface waters: Kinetic study and mathematical simulations, Environ. Sci. Pollut. Res. 29 (28) (2022) 42231–42241.

[83] P.R. Maddigapu, A. Bedini, C. Minero, V. Maurino, D. Vione, M. Brigante, G. Mailhot, M. Sarakha, The pH-dependent photochemistry of anthraqui-none-2-sulfonate, Photochem. Photobiol. Sci. 9 (3) (2010) 323–330.

[84] P. Avetta, D. Fabbri, M. Minella, M. Brigante, V. Maurino, C. Minero, M. Pazzi, D. Vione, Assessing the phototransformation of diclofenac, clofibric acid and naproxen in surface waters: model predictions and comparison with field data, Water Res. 105 (2016) 383–394.

[85] E. De Laurentiis, C. Prasse, T.A. Ternes, M. Minella, V. Maurino, C. Minero, M. Sarakha, M. Brigante, D. Vione, Assessing the photochemical trans-formation pathways of acetaminophen relevant to surface waters: trans-formation kinetics, intermediates, and modelling, Water Res. 53 (2014) 235–248.

[86] K. McNeill, S. Canonica, Triplet state dissolved organic matter in aquatic photochemistry: reaction mechanisms, substrate scope, and photophysical properties, Environ. Sci.: Process. Impacts 18 (11) (2016) 1381–1399.

[87] K. Zhang, K.M. Parker, Halogen radical oxidants in natural and engineered aquatic systems, Environ. Sci. Technol. 52 (17) (2018) 9579–9594.

[88] T. Zeng, W.A. Arnold, Pesticide photolysis in prairie potholes: Probing pho-tosensitized processes, Environ. Sci. Technol. 47 (13) (2013) 6735–6745.

[89] K.M. Parker, W.A. Mitch, Halogen radicals contribute to photooxidation in coastal and estuarine waters, Proc. Natl. Acad. Sci. USA 113 (21) (2016) 5868–5873.

[90] M. Brigante, M. Minella, G. Mailhot, V. Maurino, C. Minero, D. Vione, Formation and reactivity of the dichloride radical (Cl$_2^{-\bullet}$) in surface waters: a modelling approach, Chemosphere 95 (2014) 464–469.

[91] W.J. Jin, F.Y. Cheng, Y. Liu, H. Yang, Y.J. Zhou, J. Qu, Y.N. Zhang, Insights into generation mechanisms of halogen radicals from excited triplet state of dissolved organic matter, Sci. Total Environ. 834 (2022) 155280.

[92] A. Treinin, I. Loeff, J.K. Hurley, H. Linschitz, Charge-transfer interactions of excited molecules with inorganic anions: the role of spin-orbit coupling in controlling net electron transfer, Chem. Phys. Lett. 95 (4–5) (1983) 333–338.

[93] X. Ma, G. Wang, L. Qin, J. Liu, B. Li, Y. Hu, H. Cheng, Z-scheme g-C$_3$N$_4$-AQ-MoO$_3$ photocatalyst with unique electron transfer channel and large reduction area for enhanced sunlight photocatalytic hydrogen production, Appl. Catal. B Environ. 288 (2021) 120025.

[94] C. Xue, P. Wang, H. Che, W. Liu, B. Liu, Y. Ao, Simultaneous organic pollutant degradation and hydrogen peroxide production by molecular-engineered carbon nitride, Appl. Catal. B Environ. 340 (2024) 123259.

[95] X. Liu, B.K. Li, Q.X. Liu, P.F. Li, F. Ling, G.X. Wang, *In vivo* and *in vitro* antiviral effect and mechanisms of rhein against nervous necrosis virus, Aquaculture 579 (2024) 740207.

[96] H. Hou, X. Zeng, X. Zhang, Production of hydrogen peroxide by photocatalytic processes, Angew. Chem. Int. Ed. 59 (40) (2020) 17356–17376.

[97] J.M. Campos Martin, G. Blanco Brieva, J.L.G. Fierro, Hydrogen peroxide syn-thesis: an outlook beyond the anthraquinone process, Angew. Chem. Int. Ed. 45 (42) (2006) 6962–6984.

[98] M.G. Ren, M. Mao, X.Y. Duan, Q.H. Song, Hydrogen peroxide synthesis by direct photoreduction of 2-ethylanthraquinone in aerated solutions, J. Photochem. Photobiol. Chem. 217 (1) (2011) 164–168.

[99] G. Xu, Y. Liang, F. Chen, Continuously photocatalytic production of H$_2$O$_2$ with high concentrations by using 2-ethylanthraquinone as photocatalyst, J. Mol. Catal. Chem. 420 (2016) 66–72.

[100] H.I. Kim, Y. Choi, S. Hu, W. Choi, J.H. Kim, Photocatalytic hydrogen peroxide production by anthraquinone-augmented polymeric carbon nitride, Appl. Catal. B Environ. 229 (2018) 121–129.

[101] G. Minsu, D.Y. Lee, J. Mun, D. Kim, H.I. Cho, B. Kim, W. Kim, G. Lee, B.S. Kim, H.I. Kim, Solar-to-hydrogen peroxide conversion of photocatalytic carbon dots with anthraquinone: Unveiling the dual role of surface functionalities, Appl. Catal. B Environ. 312 (2022) 121379.

[102] B. Gao, Z. Safaei, I. Babu, S. Iftekhar, E. Iakovleva, V. Srivastava, B. Doshi, S. Ben Hammouda, S. Kalliola, M. Sillanpaa, Modification of ZnIn$_2$S$_4$ by anthraqui-none-2-sulfonate doped polypyrrole as acceptor-donor system for enhanced photocatalytic degradation of tetracycline, J. Photochem. Photobiol. Chem. 348 (2017) 150–160.

[103] Y. Zhang, L. Wang, L. Lu, M. Liu, Z. Yuan, L. Yang, C. Liu, S. Huang, Y. Rao, Highly efficient decontamination of tetracycline and pathogen by a natural product-derived Emodin/HAp photocatalyst, Chemosphere 305 (2022) 135401.

[104] U. Alam, A. Pandey, N. Verma, An anthraquinone-integrated S-scheme-based NiTiO$_3$-g-C$_3$N$_4$ composite with enhanced hydrogen production activity, Int. J. Hydrogen Energy 48 (7) (2023) 2532–2541.

[105] W. Zhang, J. Gacs, I.W.C.E. Arends, F. Hollmann, Selective photooxidation reactions using water-soluble anthraquinone photocatalysts, ChemCatChem 9 (20) (2017) 3821–3826.

[106] K. Xiong, F. Zhang, Y. Wang, B. Zeng, X. Lang, Selective oxidation of amines powered with green light and oxygen over an anthraquinone covalent organic framework, J. Colloid Interface Sci. 643 (2023) 340–349.

[107] C. Chu, Q. Zhu, Z. Pan, S. Gupta, D. Huang, Y. Du, S. Weon, Y. Wu, C. Muhich, E. Stavitski, K. Domen, J.H. Kim, Spatially separating redox centers on 2D carbon nitride with cobalt single atom for photocatalytic H$_2$O$_2$ production, Proc. Natl. Acad. Sci. USA 117 (12) (2020) 6376–6382.

[108] S.N. Baker, G.A. Baker, Luminescent carbon nanodots: Emergent nanolights, Angew. Chem. Int. Ed. 49 (38) (2010) 6726–6744.

[109] T.H. Jeon, H. Kim, H.I. Kim, W. Choi, Highly durable photoelectrochemical H$_2$O$_2$ production via dual photoanode and cathode processes under solar simulating and external bias-free conditions, Energy Environ. Sci. 13 (6) (2020) 1730–1742.

[110] X. Zong, H. Chen, B. Seger, T. Pedersen, M.S. Dargusch, E.W. McFarland, C. Li, L. Wang, Selective production of hydrogen peroxide and oxidation of hydrogen sulfide in an unbiased solar photoelectrochemical cell, Energy Environ. Sci. 7 (10) (2014) 3347–3351.

[111] C. Tang, T. Bao, S. Li, X. Wang, H. Rao, P. She, J.S. Qin, Bioinspired 3D pene-trating structured micro-mesoporous NiCoFe-LDH@ZnIn$_2$S$_4$ Z-scheme het-erojunction for simultaneously photocatalytic H$_2$ evolution coupled with benzylamine oxidation, Appl. Catal. B Environ. 342 (2024) 123384.

[112] Z. Lu, J. Gao, S. Rao, C. Jin, H. Jiang, J. Shen, X. Yu, W. Wang, J. Yang, Q. Liu, A multifunctional membrane based on TiO$_2$/PCN-224 heterojunction with synergistic photocatalytic-photothermal activity under visible-light irradiation, Appl. Catal. B Environ. 342 (2024) 123374.

[113] X. Cheng, B. Liu, H. Zhao, H. Zhang, J. Wang, Z. Li, B. Li, Z. Chen, J. Hu, Interfacial effect between Ni$_2$P/CdS for simultaneously heightening photo-catalytic hydrogen production and lignocellulosic biomass photorefining, J. Colloid Interface Sci. 655 (2024) 943–952.

[114] X. Ma, S. Li, Z. Qu, M. Zhang, J. Qiao, X. Cui, C. Wang, J. Wang, Y. Song, A highly active Z-scheme NiGa$_2$O$_4$/anthraquinone/MoO$_3$ photocatalyst via charge transfer for sunlight photocatalytic simultaneous conversions of nitrite and sulfite, J. Ind. Eng. Chem. 78 (2019) 303–314.

[115] M. Ming, H. Yuan, S. Yang, Z. Wei, Q. Lei, J. Lei, Z. Han, Efficient red-light-

driven hydrogen evolution with an anthraquinone organic dye, J. Am. Chem. Soc. 144 (43) (2022) 19680–19684.

[116] H. Wang, L. Li, X. Li, C. He, Encapsulation of organic dyes within an electron-deficient redox metal-organic tetrahedron for photocatalytic proton reduction, Isr. J. Chem. 59 (3–4) (2019) 273–279.

[117] B.C. Hodges, E.L. Cates, J.H. Kim, Challenges and prospects of advanced oxidation water treatment processes using catalytic nanomaterials, Nat. Nanotechnol. 13 (8) (2018) 642–650.

[118] V. Dutta, A. Sudhaik, Sonu, P. Raizada, A. Singh, T. Ahamad, S. Thakur, Q.V. Le, V.H. Nguyen, P. Singh, Tailoring S-scheme-based carbon nanotubes (CNTs) mediated Ag-CuBi$_2$O$_4$/Bi$_2$S$_3$ nanomaterials for photocatalytic dyes degradation in the aqueous system, J. Mater. Sci. Technol. 162 (2023) 11–24.

[119] H. Görner, Photoinduced oxygen uptake for 9,10-anthraquinone in air-saturated aqueous acetonitrile in the presence of formate, alcohols, ascorbic acid or amines, Photochem. Photobiol. Sci. 5 (11) (2006) 1052–1058.

[120] M. Chen, Q. Cai, X. Chen, S. Huang, Q. Feng, T. Majima, R.J. Zeng, S. Zhou, Anthraquinone-2-sulfonate as a microbial photosensitizer and capacitor drives solar-to-N$_2$O production with a quantum efficiency of almost unity, Environ. Sci. Technol. 56 (8) (2022) 5161–5169.

[121] Y. Bai, A. Mellage, O.A. Cirpka, T. Sun, L.T. Angenent, S.B. Haderlein, A. Kappler, AQDS and redox-active NOM enables microbial Fe(III)-mineral reduction at cm-scales, Environ. Sci. Technol. 54 (7) (2020) 4131–4139.

[122] K. Hasegawa, P. Neta, Rate constants and mechanisms of reaction of chloride (Cl$_2^-$) radicals, J. Phys. Chem. 82 (8) (1978) 854–857.

[123] G.V. Buxton, M. Bydder, G. Arthur Salmon, J.E. Williams, The reactivity of chlorine atoms in aqueous solution. Part III. The reactions of Cl$^•$ with solutes, Phys. Chem. Chem. Phys. 2 (2) (2000) 237–245.

[124] S. Zhao, C. Chen, J. Ding, S. Yang, Y. Zang, X. Qin, X. Gao, Z. Song, N. Ren, Fabrication of AQ2S/GR composite photosensitizer for the simulated solar light-driven degradation of sulfapyridine, Environ. Sci. Ecotechnology 8 (2021) 100111.

[125] V. Cardoso, T. Rittmeyer, R.J. Correa, G.C. Brêda, R.V. Almeida, G. Simões, B.M. de França, P.N. de Azevedo, J.S. Bello Forero, Photoactive cotton fabric: synthesis, characterization and antibacterial evaluation of anthraquinone-based dyes linked to cellulose, Dyes Pigments 161 (2019) 16–23.

[126] Y. Zhu, A. Sulkanen, G.-Y. Liu, G. Sun, Daylight-active cellulose nanocrystals containing anthraquinone structures, Materials 13 (16) (2020) 3547.

[127] Q. Zhu, Y. Jin, G. Sun, K. Yan, D. Wang, AQC functionalized CNCs/PVA-co-PE composite nanofibrous membrane with flower-like microstructures for photo-induced multi-functional protective clothing, Cellulose 25 (8) (2018) 4819–4830.

[128] P. Sokkar, A. Babu, A. Kolandaswamy, F.A. Daison, M. Ramachandran, Effect of substituents on the photodynamic action of anthraquinones: EPR, computational and *in vitro* studies, Photochem. Photobiol. 98 (2022) 1426–1433.

[129] J. Dimmer, F.V. Cabral, C.P. Sabino, C.R. Silva, S.C. Núñez-Montoya, J.L. Cabrera, M.S. Ribeiro, Natural anthraquinones as novel photosentizers for antiparasitic photodynamic inactivation, Phytomedicine 61 (2019) 152894.

[130] W. Tian, C. Wang, D. Li, H. Hou, Novel anthraquinone compounds as anti-cancer agents and their potential mechanism, Future Med. Chem. 12 (7) (2020) 627–644.

[131] Z.O. Olatunde, J. Yong, C. Lu, Y. Ming, A review on shikonin and its derivatives as potent anticancer agents targeted against topoisomerases, Curr. Med. Chem. 31 (8) (2024) 920–937.

[132] R.B. Semwal, D.K. Semwal, S. Combrinck, A. Viljoen, Emodin - a natural anthraquinone derivative with diverse pharmacological activities, Phytochemistry 190 (2021) 112854.

[133] A.R. Montazerabadi, A. Sazgarnia, M.H. Bahreyni Toosi, A. Ahmadi, A. Shakeri Zadeh, A. Aledavood, Mitoxantrone as a prospective photosensitizer for photodynamic therapy of breast cancer, Photodiagnosis Photodyn. Ther. 9 (1) (2012) 46–51.

[134] T. Qun, T. Zhou, J. Hao, C. Wang, K. Zhang, J. Xu, X. Wang, W. Zhou, Anti-bacterial activities of anthraquinones: structure–activity relationships and action mechanisms, RSC Med. Chem. 14 (8) (2023) 1446–1471.

[135] Y. Liu, M.S.T. Mapa, R.L. Sprando, Liver toxicity of anthraquinones: a combined *in vitro* cytotoxicity and *in silico* reverse dosimetry evaluation, Food Chem. Toxicol. 140 (2020) 111313.

[136] X. Dong, F. Huang, Y. Wang, K. Zhang, X. Lang, Selective oxidation of sulfides by pyrene-π-anthraquinone conjugated microporous polymer photocatalysis, Mater. Today Energy 38 (2023) 101443.

[137] X. Dong, Y. Wang, F. Huang, X. Lang, Carbazole–anthraquinone conjugated microporous polymer photocatalysis for aerobic oxidative cyanation of tertiary amines irradiated by green light, Chem. Eng. J. 469 (2023) 143934.

[138] W. Lee, S. Jung, M. Kim, S. Hong, Site-selective direct C—H pyridylation of unactivated alkanes by triplet excited anthraquinone, J. Am. Chem. Soc. 143 (7) (2021) 3003–3012.

[139] P. Xu, W. Fan, P. Chen, G. Liu, Enantioselective radical trifluoromethylation of benzylic C—H bonds via cooperative photoredox and copper catalysis, J. Am. Chem. Soc. 144 (30) (2022) 13468–13474.

[140] L. Wang, T. Wang, G.J. Cheng, X. Li, J.J. Wei, B. Guo, C. Zheng, G. Chen, C. Ran, C. Zheng, Direct C—H arylation of aldehydes by merging photocatalyzed hydrogen atom transfer with palladium catalysis, ACS Catal. 10 (14) (2020) 7543–7551.

[141] L. Cui, Y. Matsuaki, N. Tada, T. Miura, B. Uno, A. Itoh, Metal-free direct C—H perfluoroalkylation of arenes and heteroarenes using a photoredox organocatalyst, Adv. Synth. Catal. 355 (11–12) (2013) 2203–2207.

[142] J.I. Bardagi, I. Ghosh, M. Schmalzbauer, T. Ghosh, B. König, Anthraquinones as phohotoredox catalysts for the reductive activation of aryl halides, Eur. J. Org. Chem. 2018 (1) (2018) 34–40.

[143] C. Cai, X. Lai, Y. Wang, H. Hu, J. Song, Y. Yang, C. Wang, H. Xu, Photo-electrochemical asymmetric catalysis enables site- and enantioselective cyanation of benzylic C—H bonds, Nat. Catal. 5 (10) (2022) 943–951.

[144] P.J. Wagner, R.J. Truman, A.E. Puchalski, R. Wake, Extent of charge transfer in the photoreduction of phenyl ketones by alkylbenzenes, J. Am. Chem. Soc. 108 (24) (1986) 7727–7738.

[145] B. Yuan, D. Mahor, Q. Fei, R. Wever, M. Alcalde, W. Zhang, F. Hollmann, Water-soluble anthraquinone photocatalysts enable methanol-driven enzymatic halogenation and hydroxylation reactions, ACS Catal. 10 (15) (2020) 8277–8284.

[146] Q. Li, X. Lan, G. An, L. Ricardez Sandoval, Z. Wang, G. Bai, Visible-light-responsive anthraquinone functionalized covalent organic frameworks for metal-free selective oxidation of sulfides: effects of morphology and structure, ACS Catal. 10 (12) (2020) 6664–6675.

[147] Z. Wang, L. Zeng, C. He, C. Duan, Metal−organic framework-encapsulated anthraquinone for efficient photocatalytic hydrogen atom transfer, ACS Appl. Mater. Interfaces 14 (6) (2022) 7980–7989.

[148] H. Yuan, J. Du, M. Ming, Y. Chen, L. Jiang, Z. Han, Combination of organic dye and iron for CO$_2$ reduction with pentanuclear Fe$_2$Na$_3$ purpurin photocatalysts, J. Am. Chem. Soc. 144 (10) (2022) 4305–4309.

[149] N. An, L. Zhou, W. Li, X. Yuan, L. Zhao, J. Huang, Y. Zhang, H. She, L. Wang, Q. Wang, Multifunctional polymer coating cooperated with γ-Fe$_2$O$_3$ for boosting photoelectrochemical water oxidation, Appl. Catal. B Environ. 318 (2022) 121869.

[150] Q. Lei, H. Yuan, J. Du, M. Ming, S. Yang, Y. Chen, J. Lei, Z. Han, Photocatalytic CO$_2$ reduction with aminoanthraquinone organic dyes, Nat. Commun. 14 (1) (2023) 1087.

[151] Y. Wang, G. Ji, W. Ye, F. Zhang, Y. Wang, Y. Zhao, Z. Liu, DFT-assisted design of D−A conjugated polymers for photocatalytic reduction of carbon dioxide, ACS Sustainable Chem. Eng. 10 (29) (2022) 9460–9468.

[152] Z. Guo, S. Cheng, C. Cometto, E. Anxolabéhère Mallart, S.M. Ng, C.C. Ko, G. Liu, L. Chen, M. Robert, T.C. Lau, Highly efficient and selective photocatalytic CO$_2$ reduction by iron and cobalt quaterpyridine complexes, J. Am. Chem. Soc. 138 (30) (2016) 9413–9416.

[153] H. Yuan, B. Cheng, J. Lei, L. Jiang, Z. Han, Promoting photocatalytic CO$_2$ reduction with a molecular copper purpurin chromophore, Nat. Commun. 12 (1) (2021) 1835.

[154] A. Kumar, P. Singh, A.A.P. Khan, Q.V. Le, V.H. Nguyen, S. Thakur, P. Raizada, CO$_2$ photoreduction into solar fuels via vacancy engineered bismuth-based photocatalysts: selectivity and mechanistic insights, Chem. Eng. J. 439 (2022) 135563.

[155] Y. Zhu, Z. He, Y. Choi, H. Chen, X. Li, B. Zhao, Y. Yu, H. Zhang, K.A. Stoerzinger, Z. Feng, Y. Chen, M. Liu, Tuning proton-coupled electron transfer by crystal orientation for efficient water oxidization on double perovskite oxides, Nat. Commun. 11 (1) (2020) 4299.

[156] D. Zhang, W. Liang, J. Yi, J. Chen, Y. Lv, T. Zhao, C. Xiao, X. Xie, W. Wu, C. Yang, Photochemical graft of γ-cyclodextrin's interior leading to *in-situ* charge-transfer complexes with unusual regioselectivity and its application in 3D photo-printing, Sci. China: Chem. 65 (6) (2022) 1149–1156.

[157] Y. Zhou, S. Zhang, F. Zheng, Q. Lu, Intrinsically black polyimide with retained insulation and thermal properties: a black anthraquinone derivative capable of linear copolymerization, Macromolecules 54 (20) (2021) 9307–9318.

[158] C. Zhao, X. Kong, S. Shuang, Y. Wang, C. Dong, An anthraquinone-imidazole-based colorimetric and fluorescent sensor for the sequential detection of Ag$^+$ and biothiols in living cells, Analyst 145 (8) (2020) 3029–3037.

[159] L. Hou, X. Kong, Y. Wang, J. Chao, C. Li, C. Dong, Y. Wang, S. Shuang, An anthraquinone-based highly selective colorimetric and fluorometric sensor for sequential detection of Cu^{2+} and S^{2-} with intracellular application, J. Mater. Chem. B 5 (45) (2017) 8957–8966.

[160] N.O.d. Farias, A.F.d. Albuquerque, A. dos Santos, G.C.F. Almeida, H.S. Freeman, R. Räisänen, G.d.A. Umbuzeiro, Is natural better? An ecotoxicity study of anthraquinone dyes, Chemosphere 343 (2023) 140174.

[161] Y. Wang, J. Chen, L. Ge, D. Wang, X. Cai, L. Huang, C. Hao, Experimental and theoretical studies on the photoinduced acute toxicity of a series of anthraquinone derivatives towards the water flea (*Daphnia magna*), Dyes Pigments 83 (3) (2009) 276–280.

[162] L. Xia, W. Huo, H. Zhang, K. Xu, Y. Qing, F. Chu, C. Zou, H. Liu, Z.a. Tan, Enhancing the cycling stability of anthraquinone-based redox flow batteries by using thermally oxidized carbon felt, ACS Appl. Energy Mater. 5 (2) (2022) 1984–1991.

[163] H. Lu, J.T. Zhou, J. Wang, W.L. Si, H. Teng, G.F. Liu, Enhanced biodecolorization of azo dyes by anthraquinone-2-sulfonate immobilized covalently in polyurethane foam, Bioresour. Technol. 101 (18) (2010) 7185–7188.

[164] S.Z. Yuan, H. Lu, J. Wang, J.T. Zhou, Y. Wang, G.F. Liu, Enhanced bio-decolorization of azo dyes by quinone-functionalized ceramsites under saline conditions, Process Biochem. 47 (2) (2012) 312–318.

[165] F.J. Cervantes, A. Garcia Espinosa, M.A. Moreno Reynosa, J.R. Rangel Mendez, Immobilized redox mediators on anion exchange resins and their role on the reductive decolorization of azo dyes, Environ. Sci. Technol. 44 (5) (2010) 1747–1753.

[166] H.K. Zhang, X.K. Hu, Catalytic reduction of NACs by nano Fe$_3$O$_4$/quinone composites in the presence of a novel marine exoelectrogenic bacterium

under hypersaline conditions, RSC Adv. 7 (20) (2017) 11852−11861.

[167] L. Zhao, J. Yu, C. Xing, Z. Ullah, C. Yu, S. Zhu, M. Chen, W. Li, Q. Li, L. Liu, Nanopore confined anthraquinone in MOF-derived N-doped microporous carbon as stable organic cathode for lithium-ion battery, Energy Storage Mater. 22 (2019) 433−440.

[168] L. Li, H. Yang, X. Wang, Y. Ma, W. Ou, H. Peng, G. Ma, An anthraquinone-based covalent organic framework for highly reversible aqueous zinc-ion battery cathodes, J. Mater. Chem. A 11 (47) (2023) 26221−26229.

[169] L. Chu, L. Cang, Z. Sun, X. Wang, G. Fang, J. Gao, Efficient hydrogen peroxide electrosynthesis using anthraquinone covalently bonded CNT on super-hydrophobic air breathing cathode, J. Clean. Prod. 378 (2022) 134578.

[170] B. Song, M. Chen, G. Zeng, J. Gong, M. Shen, W. Xiong, C. Zhou, X. Tang, Y. Yang, W. Wang, Using graphdiyne (GDY) as a catalyst support for enhanced performance in organic pollutant degradation and hydrogen production: a review, J. Hazard Mater. 398 (2020) 122957.

[171] Y. Li, M. Zhang, H. Han, B. Zhang, J.B. Matson, D. Chen, W. Li, Y. Wang, Peptide-based supramolecular photodynamic therapy systems: from rational molecular design to effective cancer treatment, Chem. Eng. J. 436 (2022) 135240.

[172] J. Liu, Q. Ma, Z. Huang, G. Liu, H. Zhang, Recent progress in graphene-based noble-metal nanocomposites for electrocatalytic applications, Adv. Mater. 31 (9) (2019) 1800696.

[173] A.K. Geim, K.S. Novoselov, The rise of graphene, Nat. Mater. 6 (3) (2007) 183−191.

[174] F. Bonaccorso, L. Colombo, G. Yu, M. Stoller, V. Tozzini, A.C. Ferrari, R.S. Ruoff, V. Pellegrini, Graphene, related two-dimensional crystals, and hybrid systems for energy conversion and storage, Science 347 (6217) (2015) 1246501.

[175] R. Kumar, A. Sudhaik, Sonu, P. Raizada, V.H. Nguyen, Q. Van Le, T. Ahamad, S. Thakur, C.M. Hussain, P. Singh, Integrating K and P co-doped g-C₃N₄ with ZnFe₂O₄ and graphene oxide for S-scheme-based enhanced adsorption coupled photocatalytic real wastewater treatment, Chemosphere 337 (2023) 139267.

[176] C. Huang, C. Li, G. Shi, Graphene based catalysts, Energy Environ. Sci. 5 (10) (2012) 8848−8868.

[177] C. Wang, W. Dong, A. Li, D.G. Atinafu, G. Wang, Y. Lu, The reinforced photothermal effect of conjugated dye/graphene oxide-based phase change materials: fluorescence resonance energy transfer and applications in solar-thermal energy storage, Chem. Eng. J. 428 (2022) 130605.

[178] H. Lu, H.K. Zhang, J. Wang, J.T. Zhou, Y. Zhou, A novel quinone/reduced graphene oxide composite as a solid-phase redox mediator for chemical and biological Acid Yellow 36 reduction, RSC Adv. 4 (88) (2014) 47297−47303.

[179] H. Zhang, H. Lu, J. Wang, J. Zhou, M. Sui, Cr(VI) reduction and Cr(III) immo-bilization by *acinetobacter* sp. HK-1 with the assistance of a novel quinone/graphene oxide composite, Environ. Sci. Technol. 48 (21) (2014) 12876−12885.

[180] Y. Zhou, H. Lu, J. Wang, J. Zhou, X. Leng, G. Liu, Catalytic performance of quinone and graphene-modified polyurethane foam on the decolorization of azo dye Acid Red 18 by *Shewanella* sp RQs-106, J. Hazard Mater. 356 (2018) 82−90.

[181] K. Kalinathan, D.P. DesRoches, X.R. Liu, P.G. Pickup, Anthraquinone modified carbon fabric supercapacitors with improved energy and power densities, J. Power Sources 181 (1) (2008) 182−185.

[182] G. Pognon, T. Brousse, L. Demarconnay, D. Belanger, Performance and sta-bility of electrochemical capacitor based on anthraquinone modified acti-vated carbon, J. Power Sources 196 (8) (2011) 4117−4122.

[183] M. Pandurangappa, N.S. Lawrence, R.G. Compton, Homogeneous chemical derivatisation of carbon particles: a novel method for funtionalising carbon surfaces, Analyst 127 (12) (2002) 1568−1571.

[184] J.M. Seinberg, M. Kullapere, U. Mäeorg, F.C. Maschion, G. Maia, D.J. Schiffrin, K. Tammeveski, Spontaneous modification of glassy carbon surface with anthraquinone from the solutions of its diazonium derivative: an oxygen reduction study, J. Electroanal. Chem. 624 (1) (2008) 151−160.

[185] J. Lee, S. Kim, Mediator-free solar energy conversion by the artificially installed thylakoid membrane on the functionalized electrode, Electrochem. Commun. 49 (2014) 55−59.

[186] H. Lu, Y. Zhou, Z. Fu, X. Wang, J. Zhou, W. Guo, Mutual interaction between the secreted flavins and immobilized quinone in anaerobic removal of high-polarity aromatic compounds containing nitrogen by *Shewanella* sp. RQs-106, J. Hazard Mater. 431 (2022) 128595.

[187] G. Maia, F.C. Maschion, S.T. Tanimoto, K. Vaik, U. Mäeorg, K. Tammeveski, Attachment of anthraquinone derivatives to glassy carbon and the electro-catalytic behavior of the modified electrodes toward oxygen reduction, J. Solid State Electrochem. 11 (10) (2007) 1411−1420.

[188] G. Zhang, F. Yang, M. Gao, L. Liu, Electrocatalytic behavior of the bare and the anthraquinonedisulfonate/polypyrrole composite film modified graphite cathodes in the electro-fenton system, J. Phys. Chem. C 112 (24) (2008) 8957−8962.

[189] S. Eigler, A. Hirsch, Chemistry with graphene and graphene oxi-de—challenges for synthetic chemists, Angew. Chem. Int. Ed. 53 (30) (2014) 7720−7738.

[190] L. Madec, A. Bouvree, P. Blanchard, C. Cougnon, T. Brousse, B. Lestriez, D. Guyomard, J. Gaubicher, In situ redox functionalization of composite electrodes for high power-high energy electrochemical storage systems via a non-covalent approach, Energy Environ. Sci. 5 (1) (2012) 5379−5386.

[191] G.E. Yuan, G.Q. Zhang, J. Chen, L. Fu, L. Xu, F.L. Yang, The electrochemical

[192] Z. Chen, J.F. Zhang, K.Z. Han, C.Y. Yang, X.L. Jiang, D. Fu, Q.B. Li, Y.P. Wang, A novel AQDS-rGO composite to enhance the bioreduction of As(v)/Fe(III) from the flooded arsenic-rich soil, RSC Adv. 7 (49) (2017) 31075−31084.

[193] H. Zhou, A. Uysal, D.M. Anjos, Y. Cai, S.H. Overbury, M. Neurock, J.K. McDonough, Y. Gogotsi, P. Fenter, Understanding defect-stabilized noncovalent functionalization of graphene, Adv. Mater. Interfac. 2 (17) (2015) 1500277.

[194] M. Boota, C. Chen, M. Bécuwe, L. Miao, Y. Gogotsi, Pseudocapacitance and excellent cyclability of 2,5-dimethoxy-1,4-benzoquinone on graphene, Energy Environ. Sci. 9 (8) (2016) 2586−2594.

[195] Q. Li, X. Qin, Y. Luo, W. Lu, G. Chang, A.M. Asiri, A.O. Al Youbi, X. Sun, One-pot synthesis of Ag nanoparticles/reduced graphene oxide nanocomposites and their application for nonenzymatic H₂O₂ detection, Electrochim. Acta 83 (2012) 283−287.

[196] A. Yang, J. Li, C. Zhang, W. Zhang, N. Ma, One-step amine modification of graphene oxide to get a green trifunctional metal-free catalyst, Appl. Surf. Sci. 346 (2015) 443−450.

[197] L. Su, L. Shu, B. Shi, Y. Hang, J. Huang, Construction of enhanced photo-stability anthraquinone-type nanovesicles based on a novel two-step su-pramolecular assembly strategy and their application on multiband laser-responsive composites, ACS Appl. Mater. Interfaces 13 (36) (2021) 43458−43472.

[198] Z. Song, Y. Qian, M.L. Gordin, D. Tang, T. Xu, M. Otani, H. Zhan, H. Zhou, D. Wang, Polyanthraquinone as a reliable organic electrode for stable and fast lithium storage, Angew. Chem. Int. Ed. 54 (47) (2015) 13947−13951.

[199] A. Molina, N. Patil, E. Ventosa, M. Liras, J. Palma, R. Marcilla, New anthraquinone-based conjugated microporous polymer cathode with ultra-high specific surface area for high-performance lithium-ion batteries, Adv. Funct. Mater. 30 (6) (2020) 1908074.

[200] M. Yu, X. Yu, J. Hu, C. Tang, C. Fan, In-situ polymerization of an organic cathode for highly efficient Li-ion batteries, J. Energy Storage 74 (2023) 109575.

[201] T. Yamamoto, H. Etori, Poly(anthraquinone)s having a π-conjugation system along the main chain. Synthesis by organometallic polycondensation, redox behavior, and optical properties, Macromolecules 28 (9) (1995) 3371−3379.

[202] L. Zhong, Z. Fang, C. Shu, C. Mo, X. Chen, D. Yu, Redox donor−acceptor conjugated microporous polymers as ultralong-lived organic anodes for rechargeable air batteries, Angew. Chem. Int. Ed. 60 (18) (2021) 10164−10171.

[203] X. Xu, Y. Sui, W. Chen, G. Zhou, Y. Li, H. Zhong, H.-R. Wen, Anthraquinone-based conjugated polymers containing dual oxidation centers for photocatalytic H₂O₂ Production from H₂O and O₂ under visible-light irradi-ation, ACS Appl. Polym. Mater. 5 (9) (2023) 7571−7580.

[204] F. Lv, S. Xiong, J. Zhang, X. Wang, J. Chu, R. Zhang, M. Gong, B. Wu, G. Liu, W. Luo, Enhanced electrochromic properties of 2,6-diaminoanthraquinone and 1,3,5-triformylresorcinol (DAAQ-TFP) covalent organic framework/functionalized graphene oxide composites containing anthraquinone active unit, Electrochim. Acta 398 (2021) 139301.

[205] D. Lei, J. Xue, X. Peng, S. Li, Q. Bi, C. Tang, L. Zhang, Oxalate enhanced syn-ergistic removal of chromium(VI) and arsenic(III) over ZnFe₂O₄/g-C₃N₄: Z-scheme charge transfer pathway and photo-Fenton like reaction, Appl. Catal. B Environ. 282 (2021) 119578.

[206] C. Feng, Z. Lu, Y. Zhang, Q. Liang, M. Zhou, X. Li, C. Yao, Z. Li, S. Xu, A magnetically recyclable dual Z-scheme GCNQDs-CoTiO₃/CoFe₂O₄ com-posite photocatalyst for efficient photocatalytic degradation of oxytetracy-cline, Chem. Eng. J. 435 (2022) 134833.

[207] S.Y. Zhao, C.X. Chen, J. Ding, S.S. Yang, Y.N. Zang, N.Q. Ren, One-pot hydro-thermal fabrication of BiVO₄/Fe₃O₄/rGO composite photocatalyst for the simulated solar light-driven degradation of Rhodamine B, Front. Environ. Sci. Eng. 16 (3) (2022) 36.

[208] S. Wang, D. Li, C. Yang, G. Sun, J. Zhang, Y. Xia, C. Xie, G. Yang, M. Zhou, W. Liu, A novel method for the synthesize of nanostructured MgFe₂O₄ photocatalysts, J. Sol. Gel Sci. Technol. 84 (1) (2017) 169−179.

[209] Y.M. Wang, K.M. Mo, X. Luo, R.Q. Xia, J.Y. Song, G.H. Ning, D. Li, An anthraquinone-based Cu(I) cyclic trinuclear complex for photo-catalyzing C-C coupling reactions, Sci. China: Chem. 66 (12) (2023) 3525−3531.

[210] J. Zhou, S. Deng, L. Liu, Y. Lan, C. Chen, Three-dimensional blocky sponge based CoMoO₄ catalyst activates peroxymonosulfate to degrade sulfadime-thoxine: a remedy for ready-made catalysts to achieve convenient and continuous operation, Chem. Eng. J. 451 (2023) 138754.

[211] G. Fan, C. Cai, Z. Chen, J. Luo, B. Du, S. Yang, J. Wu, Visible-light-drivenself-floating Ag₂MoO₄/TACN@LF photocatalyst inactivation of *Microcystis aeru-ginosa*: performance and mechanisms, J. Hazard Mater. 441 (2023) 129932.

[212] Q. Ye, H. Wu, J. Li, Y. Huang, M. Zhang, Q. Yi, B. Yan, Preparation of 1,8-dichloroanthraquinone/graphene oxide/poly (vinylidene fluoride) (1,8-AQ/GO/PVDF) mediator membrane and its application to catalyzing biodegra-dation of azo dyes, Ecotoxicol. Environ. Saf. 268 (2023) 115681.

[213] J. Pan, D. Hua, Y. Hong, X. Cheng, F. Guo, K. Bing Tan, Z. Zhong, G. Zhan, Design of hybrid g-C₃N₄/GO/MCE photocatalytic membranes with enhanced separation performance under visible-light irradiation, Chem. Eng. J. 466 (2023) 143164.

[214] F. Zhang, Y.H. Li, J.Y. Li, Z.R. Tang, Y.J. Xu, 3D graphene-based gel

photocatalysts for environmental pollutants degradation, Environ. Pollut. 253 (2019) 365−376.

[215] F. Li, X. Lan, L. Wang, X. Kong, P. Xu, Y. Tai, G. Liu, J. Shi, An efficient photocatalyst coating strategy for intimately coupled photocatalysis and biodegradation (ICPB): powder spraying method, Chem. Eng. J. 383 (2020) 123092.